國 立 交 通 大 學

電控工程研究所

碩士論文

強健性與可靠度控制在電動載具上之研究

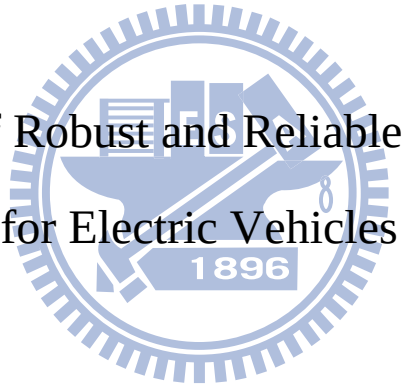

Study of Robust and Reliable Control

for Electric Vehicles

研 究 生：魏源廷

指導教授：梁耀文　博士

中 華 民 國　九 十 九 年 七 月

強健性與可靠度控制在電動載具上之研究

Study of Robust and Reliable Control for Electric Vehicles

研 究 生：魏源廷　　Student: Yuan-Tin Wei

指導教授：梁耀文 博士　　Advisor: Dr. Yew-Wen Liang

國立交通大學電控工程研究所

碩士論文

A Thesis

Submitted to institute of Electrical and Control Engineering

College of Electrical Engineering and Computer Science

National Chiao Tung University

In Partial Fulfillment of the Requirements

For the Degree of Master

In

Electrical and Control Engineering

July 2010

Hsinchu, Taiwan, Republic of China

中 華 民 國 九 十 九 年 七 月

強健性與可靠度控制在電動載具上之研究

研究生：魏源廷　　指導教授：梁耀文 博士

國立交通大學電控工程研究所

摘要

本論文首先針對電動載具系統具有不確定參數與外在干擾提出強健控制方法，利用State Dependent Riccati Equation設計法可預測系統性能的特性，積分型順滑模控制具有強健性及擁有額外設計自由度等優點來提升電動載具煞車系統之強健性，並且應用在三輪載具，模擬結果顯示了所提之結合方法可以提升系統性能。除此之外，由於電動載具對於行車安全之需求，本論文也利用了順滑模可靠度控制與錯誤偵測與估測機制針對當部分輪胎制動器完全損壞時，提升電動載具變換車道時的操控性。模擬結果顯示了，當一個、兩個或三個輪胎制動器完全損壞時，電動載具仍能達到良好的可靠度性能。

Study of Robust and Reliable Control for Electric Vehicles

Student: Yuan-Tin Wei Advisor: Dr. Yew-Wen Liang

Institute of Electrical and Control Engineering

National Chiao Tung University

ABSTRACT

In this thesis, we first address the issues regarding the robust stabilization of a class of nonlinear uncertain systems using a combined scheme. The scheme consists of the state-dependent Riccati equation (SDRE) technique for the control of nominal systems and the integral sliding mode control (ISMC) strategy to compensate for the error when the system state deviates from the nominal system trajectory. It is shown that the state of the uncertain system using the combined scheme and that of the nominal system under the SDRE scheme are identical when the uncertainties are of the matched type. These analytic results are also applied to the brake control of a three-wheeled vehicle. Simulation results show that the control under the combined scheme could be intelligently adjusted so that the yaw rate and lateral velocity is as small as possible. Second, we deal with the reliable issues of yaw rate tracking for electric vehicles using yaw moment control strategy. The presented reliable controllers are organized via the sliding mode control technique. As a result, this reliable scheme is robust and is shown to be able to tolerate some of the actuators' faults. Simulation results demonstrate the benefits of the approach.

誌謝

感謝許多人的關心與協助，使本論文能夠順利完成。首先特別要感謝指導教授梁耀文博士的用心指導，感謝老師兩年來細心與耐心的指導及對我孜孜不倦的教誨，使我不僅在研究過程中受益良多，且在待人處世各方面有許多成長。同時也要感謝口試委員鄧清政博士、廖德誠博士和徐勝均博士給予建設性的建議與指導使得本論文更臻完備。此外，感謝當我在台灣科技大學求學時，時常鼓勵我的黃世欽博士與黃安橋博士，由於你們的鼓勵，當我在研究上遇到瓶頸時，依然能夠保持活力與自信面對與處理複雜的問題。

接下來要感謝王士昕學長、丁立偉學長、吳家榮學長以及徐勝均學長在我遇到困難時能給予適時的幫助與鼓勵。謝謝實驗室的同學宜展、立岡和旭志，學弟智強、君豪、榮人以及偉庭使我兩年研究生涯多采多姿充滿回憶。謝謝你們的關懷與照顧，沒有你們的幫忙，論文不可能順利完成。

最後要感謝我的家人的大力支持與鼓勵，讓我可以無後顧之憂的在學業上勇往直前，更要感謝在交大求學生涯中陪伴著我的好友佳穗，謝謝你們，謹將此論文獻給你們。

TABLE OF CONTENTS

ABSTRACT (Chinese) i

ABSTRACT (English) ii

ACKNOWLEDGEMENT iii

TABLE OF CONTENTS iv

LIST OF TABLES vi

LIST OF FIGURES vii

1. INTRODUCTION 1

1.1. Motivation 1

1.2. Outline 5

2. PRELIMINARIES 6

2.1. State Dependent Riccati Equation 6

2.2. Integral Sliding Mode Control 7

2.3. Sliding Mode Control Design 9

2.4. Burckhardt Tire Friction Model 11

2.5 Magic Formula for Longitudinal and Lateral Force 12

3. AN INTELLIGENT SDRE AND ISMC COMBINED SCHEME WITH APPLICATION TO VEHICLE BRAKE CONTROL 15

3.1. Problem Formulation 15

3.2. Controller Design 16

3.2.1. SDRE Design for Nominal System 16

3.2.2. ISMC Design for the Compensation of Uncertainties 17

3.3. Simulation Results 19

3.3.1. Vehicle dynamics 19

3.3.2. Employment of the Combined Scheme 22

3.3.3. Simulation Results..... 23

APPENDIX 3.A..... 29

4. STUDY OF RELIABLE YAW MOMENT CONTROL FOR ELECTRIC VEHICLE..... 31

4.1. Problem Formulation 31

4.2. Reliable Controller Design…..... 33

4.2.1. Output tracking formulation……..……. 33

4.2.2. SMC reliable design……..…….. 34

4.2.3. FDD mechanism…….……..…….. 36

4.3. Simulation Results 37

4.3.1. One actuator fault…… 38

4.3.2. Two actuator faults……..…….. 39

4.3.3. Three actuator faults……..……. 40

5. CONCLUSIONS AND SUGGESTIONS FOR FURTHER RESEARCH….... 48

REFERENCES 50

LIST OF TABLES

Table 2.1. Parameters for friction coefficient characteristics (Burckhardt Tire Friction Model)……..... 12

Table 2.2. Magic Formula coefficient…..... 13

LIST OF FIGURES

Figure 2.1. Typical friction coefficient..... 12

Figure 2.2. Longitudinal force use Magic Formula..... 13

Figure 2.3. Cornering force use Magic Formula…..... 14

Figure 3.1. Three wheeled vehicle model……..... 20

Figure 3.2. Time history of the first four system states..... 25

Figure 3.3. Time history of the last three system states..... 26

Figure 3.4. Time history of the four sliding variables for SDRE+ISMC scheme..... 26

Figure 3.5. Time history of the four control inputs…..... 27

Figure 3.6. Time history of the first four system states…….. 27

Figure 3.7. Time history of the last three system states……..…..... 28

Figure 3.8. Time history of the four sliding variables for SDRE+ISMC scheme…….. 28

Figure 3.9. Time history of the four control inputs ……..…..... 29

Figure 4.1. Four wheeled vehicle model……..... 31

Figure 4.2. Time histories of (a) longitudinal velocity, (b) body side slip angle, (c) yaw rate and (d) output tracking error for one actuator fault..... 42

Figure 4.3. Time histories of (a) front-right, (b) front-left, (c) rear-right and (d) rear-left wheel angular speeds for one actuator fault…..... 43

Figure 4.4. (a) Residual signals; (b) alarm signal; (c) controls of RSMC and (d) Controls of SMC for one actuator fault…..... 43

Figure 4.5. Sliding variables of (a) RSMC and (b) SMC schemes for one actuator fault.. 44

Figure 4.6. Time histories of (a) longitudinal velocity, (b) body side slip angle, (c) yaw rate and (d) output tracking error for two actuator faults...…….. 44

Figure 4.7. Time histories of (a) front-right, (b) front-left, (c) rear-right and (d) rear-left wheel angular speeds for two actuator faults..... 45

Figure 4.8. (a) Residual signals; (b) alarm signal; (c) controls of RSMC and (d) Controls of SMC for two actuator faults..... 45
Figure 4.9. Sliding variables of (a) RSMC and (b) SMC schemes for two actuator faults 46
Figure 4.10. Time histories of (a) longitudinal velocity, (b) body side slip angle, (c) yaw rate and (d) output tracking error for three actuator faults..... 46
Figure 4.11. Time histories of (a) front-right, (b) front-left, (c) rear-right and (d) rear-left wheel angular speeds for three actuator fauls..... 47
Figure 4.12. (a) Residual signals; (b) alarm signal; (c) controls of RSMC and (d) Controls of SMC for three actuator faults…… 47
Figure 4.13. Sliding variables of (a) RSMC and (b) SMC schemes for three actuator faults..... 48

CHAPTER ONE
INTRODUCTION

1.1 Motivation

Recently, electric vehicles have achieved remarkable driving performance and has strong incentives of energy efficiency. The advantages of Electric Vehicle (EV) can be summarized as follows [15]:

1. Torque generation of an electric motor is fast and precise. The electric motor's torque response is several milliseconds, 10-100 times as fast as that of the internal combustion engine or hydraulic braking system. Because a motor can generate both acceleration or deceleration torque, therefore, the electric motor's can be integrated high performance antilock braking system and traction control system with minor feedback control.

2. A motor can be attached to each wheel. We can distribute motor location to enhance the performance of Vehicle Stability Control (VSC) such as Direct Yaw Control (DYC). It is not allowed for an Internal Combustion engine Vehicle (ICV) to use four engines, however, EV is permitted to insert four motors without increase significantly cost.

3. Motor torque can be measured easily. This advantage will contribute greatly to application of new control strategies based on road condition estimation.

To improve the safety of the driver and passengers without sacrificing the stability and steering ability of a vehicle, an antilock braking system (ABS) had been proposed to realize maximum negative acceleration, while preventing the wheels from locking [2], [14], [19], [20], [30]. Among the existing studies, there are mainly two methods of realizing the

ABS. One method uses the slip ratio to adjust the duration of brake signal pulses, i.e., to discretely "pump" the brakes [19], [30]. The other uses the fact that the friction between the road and the tire is a nonlinear function of wheel slip to regulate the slip ratio at its optimum value so that the vehicle has maximum deceleration [2], [14], [20]. In this thesis, we uses the fact that the friction between the road and the tire is a nonlinear function of wheel slip to regulate the slip ratio at its optimum value so that the vehicle has maximum deceleration to realize the ABS.

Moreover, the studies of electric vehicles' (EVs') yaw moment control and reliable (or fault tolerant) control have attracted considerable attention [4], [8], [10], [11], [18], [24]-[28], [34]-[36], [38]-[41]. EVs are known to have many advantages [11], [38], including 1) the motor torque can be measured easily and be controlled more precisely; 2) the individual motor at each wheel can generate differential distribution of braking/driving forces between the right and the left sides of the vehicle; 3) the motor enhances the diagnostic capability of the braking system. Thus, the lateral stability of EVs can be improved significantly if an appropriate controller is organized. Among the various control designs for EVs, it was reported that the yaw moment control is one of the most effective means for active chassis control, which may considerably improve the vehicle stability and controllability [10]. The yaw moment control is also an important technique behind the vehicle dynamic control systems, especially for controlling the lateral motion of a vehicle during a severe driving maneuver [10]. From the advantages mentioned above, EVs have the ability to generate more accurate yaw moment than the conventional vehicles.

Recently, the study of nonlinear control using the state-dependent Riccati equation (SDRE) approach and the integral sliding mode control (ISMC) design have attracted considerable attention [1], [5]-[7], [31], [32]. The SDRE scheme factorizes the nonlinear drift term into a (nonunique) linear structure with state-dependent coefficient (SDC) matrices and then employs the linear quadratic regulation (LQR) technique to organize an optimal controller at every nonzero state. This adoption of the LQR strategy is intuitive, and yet provides a systematic and effective controller design. The benefits of the SDRE design also include 1) the ability to predictably address system performance through the specification of the performance index by adjusting the state and the control

weightings, for instance, the engineer may tune up the weightings on the system state to speed up the response at the expense of more control effort, 2) an extra design degree of freedom arising from the non-uniqueness of the SDC representation of the nonlinear drift term, which can be utilized to enhance controller performance and 3) the preservation of the essential system nonlinearities, as it does not truncate any system nonlinear term. Many practical and meaningful applications that are successfully performed by the SDRE design, including vehicle control, have been reported [1], [7], [31], [32]. However, due to the direct adoption of the LQR strategy at every nonzero state, the SDRE design might not robustly compensate for model uncertainties and/or disturbances, which can also be observed from the simulations in this thesis. Hence, the SDRE scheme should incorporate another robust scheme for better performance.

On the other hand, the sliding mode control (SMC) design is known to have the benefits of rapid response, easy implementation and robustness to model uncertainties and/or external disturbances [2], [3], [5], [6], [21]-[23], [33]. However, it has been reported that the resulting closed-loop system might be sensitive to uncertainties and/or disturbances during the period in which the system state has not yet reached the sliding manifold [5]. To overcome the reaching phase problem, an integral sliding mode control design, which guarantees that the system trajectories will start in the manifold from the first time instant, has been studied recently [5], [6]. In addition to the absence of a reaching phase feature, the ISMC design also maintains the above-mentioned advantages of the SMC and has the following three characteristics: 1) the matched uncertainties and/or disturbances will be completely rejected whenever the system state remains on the sliding manifold, 2) the maximum control magnitude required for ISMC is usually smaller than those of SMC designs because the maximum control magnitude of SMC designs usually occurs at the beginning of reaching phase period and 3) the states of the nominal system and the matched-type uncertain system are exactly the same if the system state stays on the sliding manifold. The last feature provides an extra degree of freedom to organize a suitable controller for the nominal system, creating a desired system state trajectory for the state of the uncertain system to follow. In light of the benefits of the SDRE and the ISMC approaches mentioned above, in this thesis, investigates the ABS controller design

issues from the ISMC viewpoint, while adopting the SDRE design for nominal system.

It is known that a control system is not to be able to operate in normal (non-faulty) situation all the time, and the repair and maintenance services are in general not able to be provided instantly. These make the reliable control issues of paramount importance. The objective of reliable control is to design an appropriate controller such that the closed-loop system can tolerate abnormal operation of specific control components and retain the overall system stability with acceptable system performance. Within the existing reliable control studies, several approaches have been presented. These approaches include the linear-matrix inequality-based approach [24], the algebraic Riccatti equation-based approach [35], the coprime factorization approach [36], the Hamilton-Jacobi (HJ)-based approach [27], and the sliding-mode control (SMC)-based approach [22], [28]. Among the aforementioned reliable control studies, only the HJ-based and the SMC-based approaches deal with reliability issues for nonlinear systems. However, because the HJ-based approach was designed under an optimal strategy, its reliable controller is inevitably dependent upon the solution of an associated HJ equation, which is, in general, difficult to solve. Although a power series method [13] may alleviate the difficulty through computer calculation, the solution obtained is only approximate, and the computational load grows quickly when the system is complicated. In contrast, the SMC reliable controllers [22] do not require the solution of any HJ equation, and they retain the advantages of conventional SMC designs. Those advantages include rapid response, easy implementation, and robustness to model uncertainties and/or external disturbances.

In EVs, a fault might happen in sensor or actuator (see e.g., [8], [34], [38], [41]) that results in hazard, such as loss of steering, loss of traction force for wheel by wheel motor, brake system and inverter failure [41]. However, due to the limit of space, a vehicle is in general not allowed to insert a backup of control component. Thus, it is important for a vehicle using its analytic redundancy to equip with a suitably fault detection and diagnosis (FDD) mechanism and an active fault tolerant controller for ensuring driving safety when fault happens. For instance, when wheel actuator(s) experiences fault, the vehicle is likely to spin and result in catastrophic situation. Thus, a yaw moment reliable controller is expected to activate for preventing possible driving instability. Two recent papers

have investigated this reliable issue from feedback linearization approach [8] and LQR scheme [41]. Though the proposed two schemes are able to enhance the driving safety, one of them only considers the linear case [41] (i.e., it considers the issue based on the linearized model at a free-rolling equilibrium point), and the mentioned two approaches require incorporating a robust scheme for better robustness performance when the EVs experience model uncertainties, measurement noises and/or external disturbances. In light of the many benefits of SMC reliable design as mentioned above, in this thesis we will study the reliable control for EVs' nonlinear model from the SMC approach viewpoint.

1.2 Outline

This thesis is organized as follows. In Chapter 2, we recall some basic concepts of state dependent Riccati equation (SDRE), integral sliding mode control, sliding mode control, Burckhardt tire friction model and Magic Formula. Chapter 3 proposes an intelligent SDRE and ISMC combined scheme with application to vehicle bake control, and the associated simulations. Chapter 4 gives detailed of reliable yaw moment control for electric vehicle. Finally, in Chapter 5, we give the conclusions and suggestions for the researches in the future.

CHAPTER TWO
PRELIMINARIES

2.1 State Dependent Riccati Equation

In this section, we recall the concepts of State Dependent Riccati Equation (SDRE) [1], [5]-[7], [31], [32].

Consider the following class of nonlinear control systems

$$\dot{\mathbf{x}} = \mathbf{f}(\mathbf{x}) + B(\mathbf{x})\mathbf{u} \tag{2.1}$$

where $\mathbf{x} \in \mathbb{R}^{\mathrm{n}}$ and $\mathbf{u} \in \mathbb{R}^{\mathrm{m}}$ denote the system and control inputs, respectively, $\mathbf{f}(\mathbf{x}) \in \mathbb{R}^{\mathrm{n}}$, $B(\mathbf{x}) \in \mathbb{R}^{\mathrm{n}\times\mathrm{m}}$ and $\mathbf{f}(\mathbf{0}) = \mathbf{0}$. In addition, we consider the following performance index

$$J = \int_0^\infty \left[\mathbf{x}^T Q(\mathbf{x})\mathbf{x} + \mathbf{u}^T R(\mathbf{x})\mathbf{u}\right] dt \tag{2.2}$$

where $Q^T(\mathbf{x}) = Q(\mathbf{x}) \geq 0$ and $R^T(\mathbf{x}) = R(\mathbf{x}) > 0$. The procedure of SDRE is summarized as follows:

- Symbolically factorize $\mathbf{f}(\mathbf{x})$ into the form of $\mathbf{f}(\mathbf{x}) = A(\mathbf{x})\mathbf{x}$, where $A(\mathbf{x}) \in \mathbb{R}^{\mathrm{n}\times\mathrm{n}}$.
- Check the stabilizability of $(A(\mathbf{x}), B(\mathbf{x}))$ and the observability of $(A(\mathbf{x}), C(\mathbf{x}))$ symbolically to ensure the solvability of the following SDRE:

$$A^T(\mathbf{x})P(\mathbf{x}) + P(\mathbf{x})A(\mathbf{x}) - P(\mathbf{x})B(\mathbf{x})R^{-1}(\mathbf{x})B^T(\mathbf{x})P(\mathbf{x}) + Q(\mathbf{x}) = 0. \tag{2.3}$$

  where $C(\mathbf{x}) \in \mathbb{R}^{\mathrm{p}\times\mathrm{n}}$ has full rank and satisfies $Q(\mathbf{x}) = C^T(\mathbf{x})C(\mathbf{x})$.

- Solve the SDRE for $P(\mathbf{x})$ to produce the SDRE controller $\mathbf{u} = -R^{-1}(\mathbf{x})B^T(\mathbf{x})P(\mathbf{x})\mathbf{x}$.

Note that the SDRE scheme to the stabilization of nonlinear control systems need to symbolically factorize the drift term in the form of $\mathbf{f}(\mathbf{x}) = A(\mathbf{x})\mathbf{x}$, and then using this $A(\mathbf{x})$

to check system's stabilizability and observability symbolically at every state for ensuring the solvability of an associated state-dependent Riccati equations. In doing so, the SDRE algorithm fully captures the nonlinearities of the system, bringing the nonlinear system to a (non-unique) linear structure having state-dependent coefficient (SDC) matrices, and minimizing a nonlinear performance index having a quadratic-like structure. Moreover, the nonuniqueness of the factorization creates extra degrees of freedom, which can be used to enhance controller performance.

2.2 Sliding Mode Control

The implementation of the Sliding Mode Control (SMC) consists of two main phases. First, we should construct the sliding surface such that the system states restricted to the sliding surface will produce the desired behavior. Second, we construct switched feedback gain which derive the plant state trajectory to the sliding surface in finite time (i.e. $\sigma^T \dot{\sigma} \leq -\eta \|s\|$ for some η ¿0) and restrict the state to sliding surface (i.e. $s = 0$ and $\dot{s} = 0$). Suppose at t_0, the state trajectory of the plant intercepts the sliding surface and a sliding mode exists for all $t > t_0$. The existence of a sliding mode implies (1)$\dot{s} = 0$, and (2)$s = 0$ for all $t > t_0$. The system's motions on the sliding surface can be given an interesting geometric interpretation, as an "averag" of the systems' dynamics on both sides of the surface. The system while in sliding mode can be written as

$$\dot{s} = 0. \tag{2.4}$$

By solving the above equation formally for the control input, we obtain an expression for u called the equivalent control, u^{eq} which can be interpreted as the continuous control law that would maintain $\dot{s} = 0$ if the dynamics were exactly known. For instance, for a system of the form

$$\ddot{x} = f + u, \quad x \in \mathbb{R}. \tag{2.5}$$

In order to be converged to a desired trajectory $x(t) \equiv x_d(t)$, we define a sliding surface $s = 0$.

$$s = (\frac{d}{dt} + \lambda)\tilde{x} = \dot{\tilde{x}} + \lambda\tilde{x}, \tag{2.6}$$

here, define the tracking error $\tilde{x} = x - x_d$. We then have

$$\dot{s} = \ddot{x} - \ddot{x}_d + \lambda\dot{\tilde{x}} = f + u - \ddot{x}_d + \lambda\dot{\tilde{x}} \tag{2.7}$$

and the system dynamics while in sliding mode is, of course,

$$u^{eq} = -f + \ddot{x}_d - \lambda\dot{\tilde{x}}. \tag{2.8}$$

Controller design is the second phase of the SMC design procedure. Here the goal is to determine switched feedback gains which derive the plant state trajectory to the sliding surface and maintain a sliding mode condition. The presumption is that the sliding surface has been designed. Among several approach (e.g. the diagonalization method and hierarchical control method), augmenting the equivalent control is one popular approach. This structure of control of system (2.5) is

$$u = u^{eq} + u^{re} \tag{2.9}$$

where u^{re} is the discontinuous or the switched part of Eq.(2.9). Consider the system (2.5), we have $u^{eq} = -f + \ddot{x}_d - \lambda\dot{\tilde{x}}$. In order to satisfy sliding condition Eq.(2.12), we add to u^{eq} a term discontinuous across the surface $s = 0$, and let

$$\begin{aligned} u &= u^{eq} + u^{re} \\ &= u^{eq} - ksgn(s) \end{aligned} \tag{2.10}$$

where sgn denotes the sign function.

$$sgn(s) = \begin{cases} 1 & \text{if } s > 0 \\ 0 & \text{if } s = 0 \\ -1 & \text{if } s < 0 \end{cases} \tag{2.11}$$

By choosing k to be a positive scalar,

$$\frac{1}{2}\frac{d}{dt}s^2 = \dot{s} \cdot s = -ksgn(s) \cdot s = -k|s|. \tag{2.12}$$

Therefore, the sliding variable s will keep at zero. Practically, Eq. (2.12) states that the squared "distance" to the surface, as measured by s^2, decrease along system trajectory. Thus, it constrains trajectories to points towards the surface $S(t)$, as illustrated in Fig.

2.1. In particular, once on the surface, the system trajectories remain on the the surface. In other words, satisfying sliding condition Eq. (2.12), makes the surface an invariant set. Furthermore, as we shall see, Eq. (2.12) also implies that some disturbances or dynamics uncertainties can be tolerated while still keeping the surface an invariant set.

2.3 Integral Sliding Mode Control

In this section, we review the concepts of integral sliding mode control scheme. First, consider the following nonlinear matched uncertainties system :

$$\dot{\mathbf{x}}(t) = \mathbf{f}(\mathbf{x}) + G(\mathbf{x})\left\{\mathbf{u} + \Delta\mathbf{d}_m\right\} \tag{2.13}$$

where $\mathbf{x} \in \mathbb{R}^{\mathrm{n}}$ is a vector of states, $\mathbf{u} \in \mathbb{R}^{\mathrm{m}}$ is a vector of control inputs. $\mathbf{f}(\mathbf{x})$ and $G(\mathbf{x})$ are known nonlinear functions. $\|\mathbf{d}_m\| \leq \gamma_m$, $\gamma > 0$ which represent the matched uncertainties. In the ISMC approach, a law of the form

$$\mathbf{u}(\mathbf{x}, t) = \mathbf{u}_0 + \mathbf{u}_1 \tag{2.14}$$

is proposed. The nominal control $\mathbf{u}_0(\mathbf{x})$ is responsible for the performance of the nominal system; $\mathbf{u}_1(\mathbf{x})$ is a discontinuous control action that rejects the perturbations by ensuring the sliding motion, design as

$$\mathbf{u}_1 = \begin{cases} \mathbf{0}, & \text{if } \sigma = \mathbf{0} \\ -\rho \cdot \frac{[DG(\mathbf{x})]^T\mathbf{s}}{\left\|[DG(\mathbf{x})]^T\mathbf{s}\right\|}, & \text{if } \sigma \neq \mathbf{0} \end{cases} \tag{2.15}$$

where $\rho > \gamma_m$. and sliding surface define as

$$\sigma(\mathbf{x}, t) = D_s\left[\mathbf{x}(t) - \mathbf{x}(t_0) - \int_{t_0}^{t}\left(\mathbf{f}(\mathbf{x}) + G(\mathbf{x}) \cdot \mathbf{u}_o\right) \cdot d\tau\right] \tag{2.16}$$

where t_0 is the initial time, $D_s \in \mathbb{R}^{\mathrm{m}\times\mathrm{n}}$, and $D_sG(\mathbf{x})$ has full rank. The term

$$\mathbf{x}(t_0) + \int_{t_0}^{t}\left(\mathbf{f}((\mathbf{x})) + \mathbf{G}(\mathbf{x}) \cdot \mathbf{u_o}\right) \cdot d\tau \tag{2.17}$$

in (2.16) can be though as a trajectory of the system in the absence of perturbations and in the presence of the nominal control $\mathbf{u}_0$, that is, as a nominal trajectory for a given initial condition $\mathbf{x}(t_0)$. With this remark in mind, $\sigma(\mathbf{x})$ can be considered a penalizing factor of the difference between the actual and the nominal trajectories, projected along

G (hence, the name projection matrix, not to be confused with a projection operator). Notice that at $t = t_0$, $s(\mathbf{x}, t) = 0$, so the system always starts at the sliding manifold.

To determine the motion equations at the sliding manifold we use the equivalent control method. The derivative of s along time is

$$\begin{aligned} \dot{s} &= D_s \cdot [\dot{\mathbf{x}} - (f(\mathbf{x}) + G(\mathbf{x})\mathbf{u}_0)] \\ &= D_s \cdot \ [(\mathbf{f}(\mathbf{x}) + G(\mathbf{x})\mathbf{u} + G(\mathbf{x})\mathbf{d}_m) - (f(\mathbf{x}) + G(\mathbf{x})\mathbf{u}_0)] \\ &= D_s G(\mathbf{x}) \cdot (\mathbf{u} + \mathbf{d}_m - \mathbf{u}_0). \end{aligned} \tag{2.18}$$

Therefore, the equivalent control $\mathbf{u}_{eq} = \mathbf{u}_0 - \mathbf{d}_m$ by solving the equation $\dot{\sigma} = 0$. By substituting $\mathbf{u}_{eq}$ for $\mathbf{u}_1$ in (2.13), we obtain the sliding dynamics (motion eqations on the sliding manifold) is

$$\dot{\mathbf{x}}_{eq} = \mathbf{f}(\mathbf{x}) + G(\mathbf{x}) \cdot \mathbf{u}_0. \tag{2.19}$$

It is found from (2.19) that the matched type uncertainties can be completely rejected, and the sliding dynamics and the nominal system dynamics are exactly the same. To prove $\mathbf{u}_1$ can maintain the sliding mode, we choose a Lyapunov function as $V = 1/2\sigma^T\sigma$. Differentiating V with respect time using with respect to time using (2.14), (2.15) and (2.18) yields

$$\begin{aligned} \dot{V} &= \sigma^T \dot{\sigma} \\ &= \sigma^T D_s G(\mathbf{x}) \cdot (\mathbf{u} + \mathbf{d}_m - \mathbf{u}_0) \\ &= \sigma^T D_s G(\mathbf{x}) \cdot \left(-\rho \cdot \frac{[D_s G(\mathbf{x})]^T \mathbf{s}}{\left\| [D_s G(\mathbf{x})]^T \mathbf{s} \right\|} + \mathbf{d}_m \right) \\ &\leq -\rho \left\| (D_s G(\mathbf{x}))^T \sigma \right\| + \|\mathbf{d}_m\| \cdot \left\| (D_s G(\mathbf{x}))^T \sigma \right\| \\ &\leq (-\rho + \gamma_m) \cdot \left\| (D_s G(\mathbf{x}))^T \sigma \right\| \\ &< 0. \end{aligned} \tag{2.20}$$

since $DG(\mathbf{x})$ is of full rank and $\sigma(\mathbf{x}(t_0), t_0) = 0$, then the controller (2.14) guarantees that the sliding mode $\sigma = 0$ can be maintained, $\forall t \in [t_0, \infty)$.

2.4 Burckhardt Tire Friction Model

The friction behavior of the wheel can be approximated with parametric characteristics, as shown in Fig. 2.2. The friction, or adhesion coefficient μ is defined as the ratio of the

frictional force in the wheel plane F_{fric} and the wheel ground contact force F_z:

$$\frac{F_{fric}}{F_z}. \tag{2.21}$$

The calculation of friction forces can be carried out using the method of Burckhard [16]:

$$\mu(\lambda) = \left(c_1 \cdot \left(1 - e^{-c_2 \cdot \lambda}\right) - c_3\lambda\right) \cdot e^{-c_4 \cdot \lambda \cdot v_{cog}} \cdot \left(1 - c_5 F_Z^2\right) \tag{2.22}$$

$$\lambda = \frac{V - R_w\omega}{max(V, R_w\omega)} \tag{2.23}$$

where c_1, c_2, and c_3 are given for various road surfaces in table 2.1. c_4 lies in the rang $0.02s/m$ to $0.04s/m$ which influence of a higher drive velocity. c_5 is the influence of a higher wheel load. c_4 and c_5 have a maximum value of 1, i.e. they lead to a reduction of the friction coefficient. In this thesis, we neglect the influence of a higher wheel load and adopt as tire friction model of vehicle brake control.

Table 2.1: Parameters for friction coefficient characteristics (Burckhardt Tire Friction Model)

	c_1	c_2	c_3
Asphalt, dry	1.2801	23.99	0.52
Asphalt, wet	0.857	33.822	0.347
Snow	0.1946	94.129	0.0646

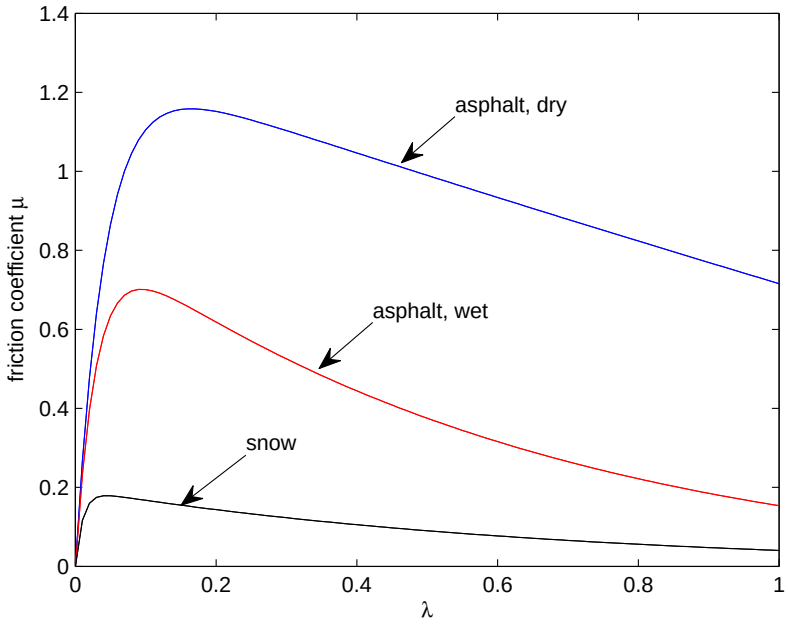

Fig. 2.1. Friction coefficient (Burckhardt Tire Friction Model)

2.5 Magic Formula for Longitudinal and Lateral Force

In general, there are many descriptions of the model for longitudinal and lateral force. In recent years, an well-known empirical method , the so-called Magic Formula, is developed for characterizing tire behavior and used in vehicle handling simulation. The Magic Formula can be used to fit experimental tire data for characterizing the relationships between the cornering face and tire slip angle or braking effort and skid. Thus, in this thesis, we adopt the Magic Formula form [37] to represent the nonlinear cornering forces. It is expressed by

$$y(x) = D \sin \left\{ C \tan^{-1} \left[Bx - E \left(Bx - \tan^{-1} Bx \right) \right] \right\} \tag{2.24}$$

where B is called the stiffness factor, C the shape factor, D the peak factor, and E the curvature factor, respectively. Where $y(x)$ represent longitudinal force f_x and lateral force f_y. When $y(x)$ represent longitudinal force f_x, then x denotes slip ratio at wheel.When $y(x)$ represent lateral force, then x denotes tire slip angle at wheel.One example of the parameter values for Magic Formula type longitudinal and cornering force are adopted from [37] as given in Table 2.2. Fig. 2.3 depicts the relationship between longitudinal force and skid. Fig. 2.4 depicts the relationship between cornering force and tire side slip

angle. In this thesis, we adopt Magic Formula as tire model of yaw moment control.

Table 2.2: Magic Formula coefficient ($F_z = 3118.3N$)

	B	C	D	E
longitudinal force	0.1664	1.65	3579.4	0.6645
lateral force	0.23	1.3	3152.9	-0.4216

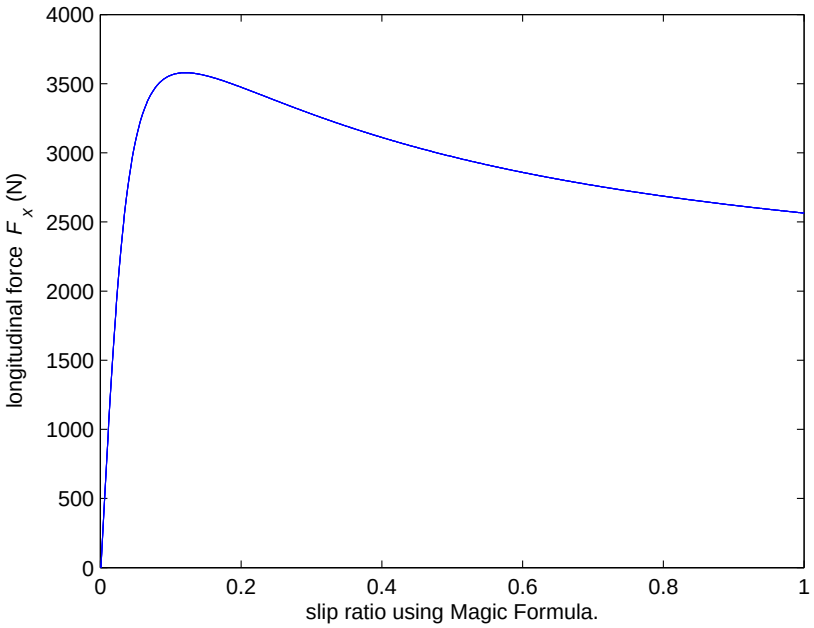

Fig. 2.2. Longitudinal force using Magic Formula

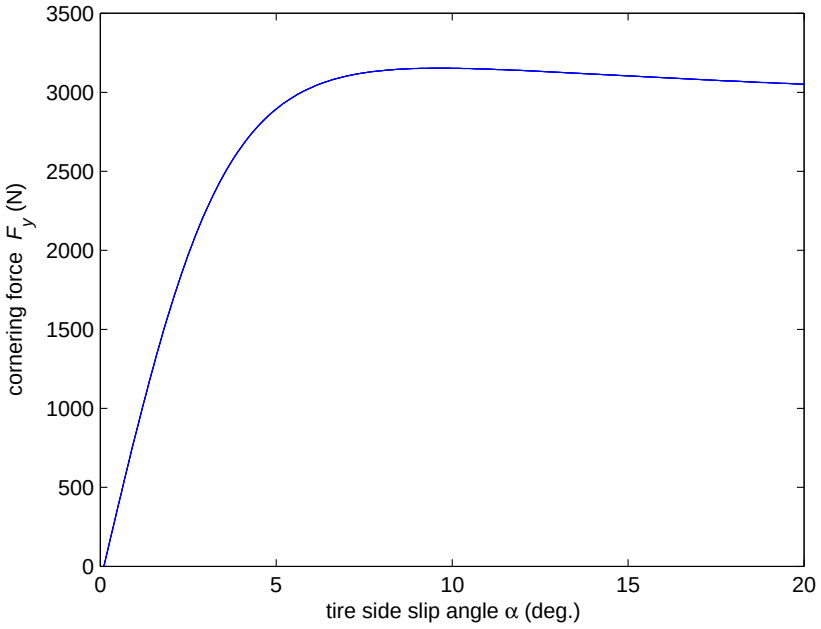

Fig. 2.3. Cornering force using Magic Formula

CHAPTER THREE
AN INTELLIGENT SDRE AND ISMC COMBINED SCHEME WITH APPLICATION TO VEHICLE BRAKE CONTROL

In this chapter, combination of the SDRE and ISMC scheme is studied and applied to vehicle brake system when actuators degradation. The organized of this chapter as follow. Section 3.2 states the problem and the main goal of this paper. Section 3.3 then describes the design of a combination of the SDRE and ISMC schemes. Section 3.4 discusses the application of the analytic results to the antilock brake control of a three-wheel vehicle system.

3.1 Problem Formulation

Consider a class of nonlinear systems described by the following equation:

$$\dot{\mathbf{x}} = \mathbf{f}(\mathbf{x}) + G(\mathbf{x})\left[(I + \Delta G)\mathbf{u} + \mathbf{d}\right] \tag{3.1}$$

where $\mathbf{x} \in \mathbb{R}^n$ and $\mathbf{u} \in \mathbb{R}^m$ denote the system states and the control inputs respectively, ΔG and $\mathbf{d}$ describe possible matched type uncertainties, $\mathbf{f}(\mathbf{x}) \in \mathbb{R}^n$ and $G(\mathbf{x}) \in \mathbb{R}^{n\times m}$. In this chapter, we assume that $G(\mathbf{x}) \neq \mathbf{0}$ for all $\mathbf{x} \neq \mathbf{0}$, and make the following three assumptions:

Assumption 3.1: The origin of the nominal system $\dot{\mathbf{x}} = \mathbf{f}(\mathbf{x}) + G(\mathbf{x})\mathbf{u}$ of System (3.1) is asymptotically stabilizable.

Assumption 3.2: $I + \Delta G \geq \kappa I$ for some $\kappa > 0$ in the sense of $\boldsymbol{\xi}^T(I + \Delta G)\boldsymbol{\xi} \geq \kappa \cdot \|\boldsymbol{\xi}\|^2$ for all $\boldsymbol{\xi} \neq \mathbf{0}$.

Assumption 3.3: There exist a positive constant ρ_g and a nonnegative function $\rho_d(\mathbf{x})$ such that $\|\Delta G\| \leq \kappa \cdot \rho_g$ and $\|\mathbf{d}\| \leq \kappa \cdot \rho_d(\mathbf{x})$.

When ΔG is a diagonal matrix and a controller has been organized, Assumption 3.2 implies that each actuator experiences no change in the output direction and only experiences degradation and/or amplification. In electrical vehicles, this degradation and/or amplification are associated with the loss of control effectiveness of steering and/or wheel torque controllers [41]. The objective of this chapter is to organize an appropriate controller to realize the regulation performance $\mathbf{x} \to \mathbf{x}_d$, where $\mathbf{x}_d$ is a nonzero constant vector.

3.2 Controller Design

Due to the many advantages of the SDRE and the ISMC approaches mentioned in the Introduction section, we combine the two schemes for the controller design in this chapter. First, the SDRE design is used for the nominal system. Then, we adopt the ISMC strategy to compensate for the error when the system state deviates from the nominal system's trajectory.

3.2.1 SDRE Design for Nominal System

To employ the SDRE approach, the regulation problem needs to be converted into the stabilization problem. For this purpose, we introduce the error state $\mathbf{e}_1 = \mathbf{x} - \mathbf{x}_d$. System (3.1) then becomes

$$\dot{\mathbf{e}}_1 = \mathbf{f}_1(\mathbf{e}_1) + G_1(\mathbf{e}_1)\left[(I + \Delta G)\mathbf{u} + \mathbf{d}\right] \tag{3.2}$$

where $\mathbf{f}_1(\mathbf{e}_1) := \mathbf{f}(\mathbf{e}_1 + \mathbf{x}_d)$ and $G_1(\mathbf{e}_1) := G(\mathbf{e}_1 + \mathbf{x}_d)$. Using this error state dynamics, the regulation problem becomes the stabilization problem, i.e., $\mathbf{x} \to \mathbf{x}_d$ if and only if $\mathbf{e}_1 \to \mathbf{0}$.

To implement the SDRE design, we assume that the quadratic performance index is given by (3.3) below:

$$J = \int_0^\infty \left[\mathbf{e}_1^T Q(\mathbf{e}_1)\mathbf{e}_1 + \mathbf{u}^T R(\mathbf{e}_1)\mathbf{u}\right] dt \tag{3.3}$$

where $Q^T(\mathbf{e}_1) = Q(\mathbf{e}_1) \geq 0$ and $R^T(\mathbf{e}_1) = R(\mathbf{e}_1) > 0$. The SDRE scheme requires the condition $\mathbf{f}_1(\mathbf{0}) = \mathbf{0}$ to factorize the drift term $\mathbf{f}_1(\mathbf{e}_1)$ in Eq. (3.2) into the form of $A_1(\mathbf{e}_1)\mathbf{e}_1$. However, there might be a state-dependent bias term, say $\mathbf{b}(\mathbf{e}_1)$, that makes $\mathbf{f}_1(\mathbf{0}) \neq \mathbf{0}$,

i.e.,

$$\mathbf{f}_1(\mathbf{e}_1) = A_1(\mathbf{e}_1)\mathbf{e}_1 + \mathbf{b}(\mathbf{e}_1) \tag{3.4}$$

with $\mathbf{b}(\mathbf{0}) \neq \mathbf{0}$. To solve this problem, we adopt a strategy from [7] to express $\mathbf{b}(\mathbf{e}_1)$ as $\mathbf{b}(\mathbf{e}_1) = \left[\frac{\mathbf{b}(\mathbf{e}_1)}{z}\right] z$ and augment the system with a stable auxiliary state z as (3.5) below:

$$\dot{z} = -k_1 z \tag{3.5}$$

where k_1 is a small positive constant that makes z change slowly, and $z(0) \neq 0$ so that $\frac{\mathbf{b}(\mathbf{e}_1)}{z}$ is smooth during the control period. With these settings, the augmented system formed by (3.5) and the nominal system of (3.2) has following form:

$$\dot{\mathbf{e}} = A(\mathbf{e})\mathbf{e} + B(\mathbf{e})\mathbf{u} \tag{3.6}$$

where $A(\mathbf{e}) = \begin{pmatrix} A_1(\mathbf{e}_1) & \frac{\mathbf{b}(\mathbf{e}_1)}{z} \\ \mathbf{0} & -k_1 \end{pmatrix}$, $B(\mathbf{e}) = \begin{pmatrix} G_1(\mathbf{e}_1) \\ \mathbf{0} \end{pmatrix}$ and $\mathbf{e} = [\mathbf{e}_1^T, z]^T$. To successfully implement the SDRE scheme, the following assumption for the existence of a unique positive definite matrix solution of an associated algebraic Riccati equation (ARE) is needed [17]:

Assumption 3.4: The pair $\left\{A(\mathbf{e}), Q^{1/2}(\mathbf{e})\right\}$ is pointwise observable and $\{A(\mathbf{e}), B(\mathbf{e})\}$ is pointwise stabilizable.

According to the SDRE design procedure, the SDRE controller then has the following form [7]

$$\mathbf{u}_0 = -R^{-1}(\mathbf{e})B^T(\mathbf{e})P(\mathbf{e})\mathbf{e} \tag{3.7}$$

where $P(\mathbf{e})$ is the unique positive definite matrix solution of the following ARE:

$$A^T(\mathbf{e})P(\mathbf{e}) + P(\mathbf{e})A(\mathbf{e}) - P(\mathbf{e})B(\mathbf{e})R^{-1}(\mathbf{e})B^T(\mathbf{e})P(\mathbf{e}) + Q(\mathbf{e}) = 0. \tag{3.8}$$

3.2.2 ISMC Design for the Compensation of Uncertainties

After selecting the nominal controller, the system might experience uncertainties, including external disturbances and actuators' output degradation and/or amplification. To compensate for these effects, we adopt the ISMC design because of its advantages, including robustness, rapid response and easy implementation.

According to the ISMC design procedure [5], [6], the sliding manifold for System (3.2) is given by the following equation:

$$\sigma = D_s \left[\mathbf{e}_1(t) - \mathbf{e}_1(t_0) - \int_{t_0}^{t} \mathbf{f}_1(\mathbf{e}_1) + G_1(\mathbf{e}_1)\mathbf{u}_0 \, d\tau \right] \tag{3.9}$$

where $D_s \in \mathbb{R}^{m \times n}$ is choose such that $D_s G_1(\mathbf{e}_1)$ has full rank and $\mathbf{u}_0$ is given by (3.7). It follows from Eqs. (3.2) and (3.9) that

$$\begin{aligned} \dot{\sigma} &= D_s \left[\dot{\mathbf{e}}_1 - \mathbf{f}_1(\mathbf{e}_1) - G_1(\mathbf{e}_1)\mathbf{u}_0 \right] \\ &= D_s G_1(\mathbf{e}_1) \left[(I + \Delta G)\mathbf{u} + \mathbf{d} - \mathbf{u}_0 \right]. \end{aligned} \tag{3.10}$$

To keep the system state on the sliding manifold, we chose the overall control law to be

$$\mathbf{u} = \mathbf{u}_0 + \mathbf{u}_1 \tag{3.11}$$

where $\mathbf{u}_0$ is given by (3.7) and

$$\mathbf{u}_1 = \begin{cases} \mathbf{0} & \text{if } \sigma = \mathbf{0}; \\ -\rho \frac{[D_s G_1(\mathbf{e}_1)]^T \sigma}{\left\| [D_s G_1(\mathbf{e}_1)]^T \sigma \right\|} & \text{otherwise} \end{cases} \tag{3.12}$$

with ρ chosen to satisfy $\rho > \rho_g \left\| \mathbf{u}_0 \right\| + \rho_d(\mathbf{e}_1)$. Although the coefficient ρ requires the information about $\mathbf{u}_0$, it can be easily obtained after the calculation of $\mathbf{u}_0$ because the upper bounds ρ_g and $\rho_d(\mathbf{e}_1)$ can be estimated offline. We then have the next result:

Theorem 3.1: Suppose that Assumptions 3.1-3.4 hold. Then the error states $\mathbf{e}_1$ given in the nominal system (3.6) with the SDRE controller and the uncertain system described by (3.2) with the control law given by (3.11)-(3.12) are identical.

proof: From Eqs. (3.10)-(3.12) and Assumptions 3.2-3.3 we have

$$\begin{aligned} \sigma^T \dot{\sigma} &= \sigma^T D_s G_1(\mathbf{e}_1) \left[(I + \Delta G)\mathbf{u}_1 - \Delta G \cdot \mathbf{u}_0 + \mathbf{d} \right] \\ &\leq \left(-\rho\kappa + \left\| \Delta G \right\| \cdot \left\| \mathbf{u}_0 \right\| + \left\| \mathbf{d} \right\| \right) \cdot \left\| [D_s G_1(\mathbf{e}_1)]^T \sigma \right\| \\ &\leq \kappa \left(-\rho + \rho_g \left\| \mathbf{u}_0 \right\| + \rho_d(\mathbf{e}_1) \right) \cdot \left\| [D_s G_1(\mathbf{e}_1)]^T \sigma \right\| \\ &< 0 \end{aligned} \tag{3.13}$$

whenever $[D_s G_1(\mathbf{e}_1)]^T \sigma \neq 0$ or $\sigma \neq \mathbf{0}$ because $D_s G_1(\mathbf{e}_1)$ is a nonsingular matrix. From (3.9), it is clear that $\sigma(\mathbf{e}_1(t_0)) = \mathbf{0}$. Thus, from (3.13), we have $\sigma(\mathbf{e}_1(t)) = 0$ for all $t \geq t_0$,

i.e., the system state remains on the sliding manifold for all $t \geq t_0$. To determine the sliding dynamics (the equations of motion on the sliding manifold), the equivalent control method is used [6]. The equivalent control is obtained by solving the equation $\dot{\sigma} = 0$ from Eq. (3.10) as follows:

$$\mathbf{u}_{eq} = (I + \Delta G)^{-1}(\mathbf{u}_0 - \mathbf{d}). \tag{3.14}$$

By substituting $\mathbf{u}_{eq}$ into (3.2), we have the sliding dynamics $\dot{\mathbf{e}}_1 = f_1(\mathbf{e}_1) + G_1(\mathbf{e}_1)\mathbf{u}_0$, which is the nominal system under the SDRE controller and the proof is completed. ■

It is found from the proof of Theorem 3.1 that the matched type uncertainties can be completely rejected, and that the sliding dynamics and the nominal system dynamics are identical. Because the system state under the ISMC scheme starts from the sliding manifold, it follows that the state trajectories of the uncertain system using the combined scheme and the nominal system under SDRE scheme are identical. Therefore, with this ISMC design the engineer can organize another optimal controller (other than the SDRE design) according to system requirements creating a desired system state trajectory for the state of the uncertain system to follow.

3.3 Simulation Results

3.3.1 Vehicle dynamics

A three wheeled vehicle (TWV) model has been described in [12]. For simplicity, we consider only the yaw plane motion, in which the simplified yaw plane vehicle model can be described as follows: the body frame, which is fixed to vehicle's center of gravity (CG), is denoted by x and y. The positive x- and y-axes represent the forward direction and right-hand side respectively, as seen by the driver. The vehicle dynamics then have the following form:

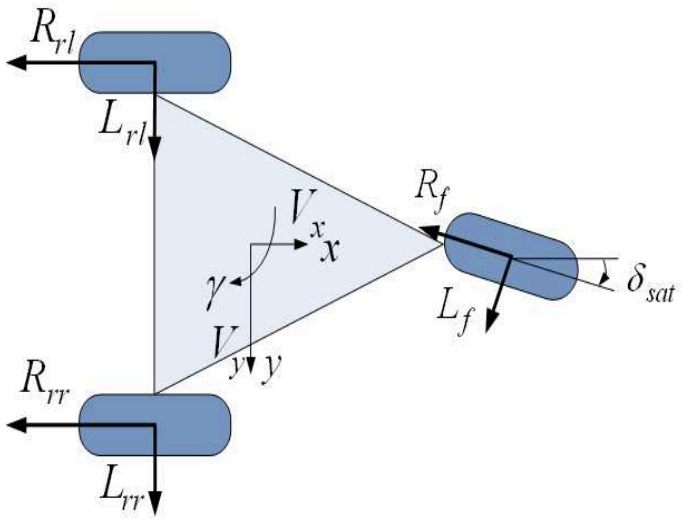

Fig. 3.1. Three wheeled vehicle model.

$$\begin{pmatrix} \dot{V}_x \\ \dot{V}_y \end{pmatrix} = \frac{1}{m}\begin{pmatrix} F_x \\ F_y \end{pmatrix} + \gamma\begin{pmatrix} V_y \\ -V_x \end{pmatrix} \tag{3.15}$$

$$\begin{aligned} J_v\dot{\gamma} &= l_1(L_f c\delta_{sat} - R_f s\delta_{sat}) - l_2(L_{rr} + L_{rl}) \\ &\quad + l_3(R_{rr} - R_{rl}) \end{aligned} \tag{3.16}$$

$$F_x = -R_f c\delta_{sat} - R_{rr} - R_{rl} - L_f s\delta_{sat} \tag{3.17}$$

$$F_y = -R_f s\delta_{sat} + L_f c\delta_{sat} + L_{rr} + L_{rl} \tag{3.18}$$

$$L_f = C_f\left(\delta_{sat} - \frac{V_y + l_1\gamma}{V_x}\right) \tag{3.19}$$

$$L_{rr} = C_{rr}\left(\frac{l_2\gamma - V_y}{V_x - l_3\gamma}\right) \tag{3.20}$$

$$L_{rl} = C_{rl}\left(\frac{l_2\gamma - V_y}{V_x + l_3\gamma}\right). \tag{3.21}$$

Here, V_x and V_y are the components of the velocity of the CG in the x- and y-directions respectively, γ denotes the angular speed about the vertical axis (z-axis), m denotes the total mass of the TWV, J_v denotes the moment of inertia in the vertical axis of the body frame, l_1 and l_2 are the longitudinal distances from the CG to the front axle and the rear axle respectively, l_3 denotes the lateral distance between CG and the left or right wheel, F_x and F_y represent the external forces acting on the body along the x- and y-axes respectively, R_α and L_α are the longitudinal and the lateral forces at each wheel between the tire patches and the road respectively, where $\alpha = f, rl, rr$ and the subscripts

f, rl and rr denote the front, the rear-left and the rear-right wheels respectively, c_α, $\alpha = f, rl, rr$, denotes the cornering stiffness for the three wheels, δ_{sat} is the actual output value of the steering wheel angle δ, defined by $\delta_{sat} = \frac{\pi}{16}$ if $\delta > \frac{\pi}{16}$; $\delta_{sat} = -\frac{\pi}{16}$ if $\delta < -\frac{\pi}{16}$; $\delta_{sat} = \frac{\pi}{16} \cdot \sin(\delta)$ if $-\frac{\pi}{16} \leq \delta \leq \frac{\pi}{16}$, and c and s denote the cosine and the sine functions respectively. In addition to the vehicle dynamics, we adopt the tire friction model from Burckhardt [14] in this chapter to simulate the antilock brake system, where R_α at each wheel can be expressed as

$$R_\alpha = \mu_\alpha N_\alpha, \ \alpha = f, rr, rl. \tag{3.22}$$

Here, $N_f = \frac{mgl_1}{L}$, $N_{rr} = \frac{mgl_2}{2L}$, $N_{rl} = \frac{mgl_2}{2L}$, $L = l_1 + l_2$, g is the acceleration of gravity and μ_α, $\alpha = f, rr, rl$, are the tire-road coefficients of friction defined by

$$\mu_\alpha = \left[c_1 \left(1 - e^{-c_2 \lambda_\alpha}\right) - c_3 \lambda_\alpha\right] \cdot e^{-c_4 \lambda_\alpha V_x} \tag{3.23}$$

where c_1, c_2, c_3 and c_4 are four parameters introduced in [14],

$$\lambda_\alpha = \begin{cases} \frac{V_x - R_w \omega_\alpha}{V_x} & \text{during braking;} \\ \frac{V_x - R_w \omega_\alpha}{r_w \omega_\alpha} & \text{during acceleration} \end{cases} \tag{3.24}$$

for $\alpha = f, rr, rl$ are the slip ratios of the three wheels, and R_w and ω_α denote the radius and the angular velocity of the wheel respectively. To study the braking performance, we consider only the slip ratio in braking mode. To achieve an optimal antilock braking performance, the wheel slip ratio is guided to track its peak value for producing maximum negative acceleration [14]. For this purpose, we differentiate λ_α and using the fact that $\dot{\omega}_\alpha = (\mu_\alpha r_w N_\alpha - T_\alpha)/J_w$ [14], yield

$$\dot{\lambda}_\alpha = \frac{\dot{V}_x (1 - \lambda_\alpha)}{V_x} + \frac{R_w T_\alpha - \mu_\alpha R_w^2 N_\alpha}{V_x J_w}, \ \alpha = f, rr, rl \tag{3.25}$$

where J_w denotes the inertia moment of wheel and T_α, $\alpha = f, rl, rr$, are the three brake torques. Finally, the vehicle model is augmented with the following steering dynamics [1]:

$$\tau \dot{\delta} \ = \ -\delta + \delta_S \tag{3.26}$$

where τ is time constant and δ_S is the steering wheel angle generated by the SDRE controller. The overall system is then described by (3.15)-(3.16) and (3.25)-(3.26).

3.3.2 Employment of the Combined Scheme

In [1], Acarman has demonstrated the efficiency of SDRE scheme in vehicle control. In this chapter, we further improve the SDRE robust performance by incorporating it with the ISMC scheme when there are model uncertainties and/or external disturbances. To employ the combined scheme, we define $\mathbf{e}_1 = [e_1, e_2, e_3, e_4, e_5, e_6, e_7]^T = [V_x, V_y, \gamma, \delta, \lambda_f - \lambda_f^*, \lambda_{rr} - \lambda_{rr}^*, \lambda_{rl} - \lambda_{rl}^*]^T$ and $\mathbf{u} = [\delta_S, T_f, T_{rr}, T_{rl}]^T$, where λ_α^*, $\alpha = f, rl, rr$, are the peak values, to be tracked, of the wheel slip ratio curves. The governing equations then have the form of (3.2), and the control objective becomes to organize an appropriate controller that effectively brings the error state $\mathbf{e}_1$ to the origin. Next, we factorize the nonlinear drift term $\mathbf{f}_1(\mathbf{e}_1)$ into a linear structure with SDC matrices. Because we require regulation performance for λ_f, λ_{rr} and λ_{rl}, the factorization of $\mathbf{f}_1(\mathbf{e}_1)$ exhibit a bias term $\mathbf{b}(\mathbf{e}_1)$, as described by Eq. (3.4). Details of an expression for $A_1(\mathbf{e}_1)$, $\mathbf{b}(\mathbf{e}_1)$ and $G_1(\mathbf{e}_1)$ given in Eq. (3.6) are presented in Appendix.

In this example we assume that the disturbance $\mathbf{d} = [0, 0, 0, 0, 0, 0, 0.5 \sin 20t]^T$ and the output of the brake torque at the rear-left wheel experiences a 40% degradation in magnitude, i.e., $[\Delta G]_{ij} = 0$ for all i, j except for $[\Delta G]_{44} = -0.4$, where $[\cdot]_{ij}$ denotes the (i, j)-entry of a matrix. The degradation might result from the abnormal operation of the inverter, braking system and/or wheel motor [41]. The vehicle parameters are assumed from [12] to be $m = 403.87$kg, $J_v = 178.54$kgm^2, $l_1 = 1.39$m, $l_2 = 0.61$m, $l_3 = 0.575$m, $C_f = 3885$N/rad, $C_{rr} = 4050$N/rad, $C_{rl} = 4050$N/rad, $R_w = 0.21$m and $J_w = 0.567$kgm^2. The time constant is set to be $\tau = 30$. The road is assumed to be dry with $c_1 = 1.2801$, $c_2 = 23.99$, $c_3 = 0.52$, $c_4 = 0.02$ and $\lambda_\alpha^* = 0.15$ for all of the three wheels [14]. The other parameters and initial state are $\kappa = 0.6$, $\rho_g = \frac{2}{3}$, $\rho_d(\mathbf{e}_1) = 0.5$, $k_1 = 10^{-3}$, $D_s = [\mathbf{0}_{4\times3}\ I_{4\times4}]$, $R = \text{diag}[10^{-1}, 1, 1, 1]$, $Q = \text{diag}[10^{-5}, 10^{-2}, 10^{-2}, 10^{-2}, 10^{6}, 10^{6}, 10^{6}]$ and $\mathbf{e}_1(0) = [30, 0, 0, 10^{-4}, -10^{-1}, -10^{-1}, -10^{-1}]^T$, where the unit of velocity is meters per second. Note that, we have promoted the weightings on the three slip ratios to make $\lambda_\alpha \to \lambda_\alpha^*$ as soon as possible and to maximize the antilock braking torque. To alleviate chatter, the control $\mathbf{u}_1$ given by (3.12) is replaced with $-\rho\frac{(D_s G_1(\mathbf{e}_1))^T \sigma}{\epsilon}$ when

$\|(D_s G_1(\mathbf{e}_1))^T \sigma\| \leq \epsilon$, and ϵ is selected to be 5×10^{-3}.

Verification of Assumption 3.4:

Finally, we need to verify Assumption 3.4 so that the SDRE scheme can be successfully implemented. Because Q is selected to be a nonsingular matrix, $(A(\mathbf{e}), Q^{\frac{1}{2}}(\mathbf{e}))$ is observable. Due to the special structure of $A(\mathbf{e})$ and $B(\mathbf{e})$ given by (3.6), $(A(\mathbf{e}), B(\mathbf{e}))$ is stabilizable if $(A_1(\mathbf{e}_1), G_1(\mathbf{e}_1))$ is controllable. To investigate the controllability of $(A_1(\mathbf{e}_1), G_1(\mathbf{e}_1))$, we introduce a matrix $M \in \mathbb{R}^{7\times 7}$ as follows: the first four columns of M are $G_1(\mathbf{e}_1)$, while the last three columns of M are taken from the last three columns of $A_1(\mathbf{e}_1)G_1(\mathbf{e}_1)$. It is found that $M = \begin{pmatrix} \mathbf{0}_{3\times 4} & M_{12} \\ M_{21} & * \end{pmatrix}$ and $M_{21} = \text{diag}[\frac{1}{\tau}, \frac{R_w}{J_w e_1}, \frac{R_w}{J_w e_1}, \frac{R_w}{J_w e_1}]$. Clearly, M_{21} is nonsingular if $e_1 \neq \mathbf{0}$ (i.e., before the vehicle is fully stopped). Since M is a block triangular matrix, we have that $(A_1(\mathbf{e}_1), G_1(\mathbf{e}_1))$ is controllable if $\det(M_{12}) \neq 0$. By direct calculation, we have $\det(M_{12}) = \frac{-2E_1E_2E_3R_w^3 l_3 s\delta_{sat}}{J_w^3 J_v m^2 e_1^3}$, where E_1, E_2 and E_3 are three nonzero scalars given in Appendix A. It follows that $(A_1(\mathbf{e}_1), G_1(\mathbf{e}_1))$ is controllable if $\sin(\delta) \neq 0$ (or $\delta \neq 0$). For $\delta = 0$, we replace the fifth column of M by the first column of $A_1^2(\mathbf{e}_1)G_1(\mathbf{e}_1)$. With this new M and the fact that $e_5 = \lambda_f - \lambda_f^*$, $e_6 = \lambda_{rr} - \lambda_{rr}^*$ and $e_7 = \lambda_{rl} - \lambda_{rl}^*$, it is found that $\det(M_{12}) = \frac{2E_2E_3l_3R_w^3}{m^3 J_v e_1^4 J_w^3} \cdot [(1-\lambda_f)(1+\frac{R_w^2}{J_w})E_1^2 + (1-\lambda_{rr})E_1E_2 + (1-\lambda_{rl})E_1E$

From (3.24), we observe that $0 \leq \lambda_\alpha \leq 1$ during braking and $\lambda_\alpha = 1$ only when the wheel is locked. Thus, $\det(M_{12}) \neq 0$ unless all the three wheels are locked (i.e., $\lambda_f = \lambda_{rr} = \lambda_{rl} = 1$). These results verify Assumption 3.4 for the period before the vehicle is fully stopped.

3.3.3 Simulation Results

Numerical results are summarized in Figs. 3.1-3.4. Among these, we consider the following three cases: the first use the SDRE scheme for the nominal system (labeled SDRE0), while the other two adopt the SDRE scheme (labeled SDRE1) and the combined scheme (labeled SDRE+ISMC) for the uncertain system (experiencing actuator's degradation and external disturbance in the actuator). It is observed from Fig. 1(a) that the longitudinal velocity converges to zero for all of the three cases. However, during the control period, the lateral velocity, the angular speed and the steering angle for SDRE1 given in Figs. 3.1(b)-3.1(d) are much larger than the other two cases, which might result

in undesirable instability. Due to the use of a saturation-type function instead of the sign-type function given in (3.12), the state trajectory of the SDRE+ISMC system deviates slightly from that of SDRE0, and it is found from simulation that the smaller the boundary layer width ϵ is, the closer the two trajectories are. From Fig. 3.3, all the sliding variables are found to be within the boundary layer. These results agree with the theoretical results. It is also observed from Fig. 3.2(c) that the performances of $\lambda_{rl} \to \lambda_{rl}^*$ are not achieved for SDRE1, which results in a worse braking performance, and the oscillation of e_7 (i.e., λ_{rl}) for SDRE1 comes from the persistent oscillation of $\mathbf{d}$. These results imply that the SDRE+ISMC scheme is more robust than the SDRE1 scheme. Finally, Fig. 3.4 shows the control efforts. Among these, the control curves of T_{rl} for the SDRE1 and SDRE+ISMC schemes have taken the degradation effect into account, i.e., those two curves describe the actual degradation torque output which is 60% of the magnitude of the designed control value. It is seen from Fig. 3.4(d) that the braking torque T_{rl} for the SDRE+ISMC systems is automatically adjusted to a level such that its degradation curve approximates that of the SDRE0 scheme, to ensure that its state responses are close to those of the SDRE0 system. The oscillations of T_{rl} for the SDRE1 and SDRE+ISMC systems resulted from the compensation for the persistent disturbance excitation. The braking torque T_{rl} for the SDRE+ISMC system is found to be a little larger than that of the SDRE1 system, since the combined scheme provides an additional control $\mathbf{u}_1$ for regulation when the system state deviates from the sliding manifold. In contrast, the required steering wheel angle δ_S for the SDRE+ISMC system is much smaller than that of the SDRE1 system. By direct calculation, the quadratic performance of the three cases has the following relation: $J_{\text{SDRE1}} = 9.2539 \times 10^5 < J_{\text{SDRE0}} = 9.2265 \times 10^5 < J_{\text{SDRE+ISMC}} = 9.0261 \times 10^5$.

Though the above simulations demonstrate the effectiveness of the combined scheme, the controls are decoupled from each other since the matrix D_s is selected to be $D_s = I$. To demonstrate the interactive relation of these actions, in the following we consider D_s has the following form:

$$D_s = \begin{bmatrix} 0 & 0 & 0 & 1 & 0 & 0 & 0 \\ 0 & 0 & 0 & 0 & 1 & 0.7 & 0.7 \\ 0 & 0 & 0 & 0 & 0.7 & 1 & 0.7 \\ 0 & 0 & 0 & 0 & 0.7 & 0.7 & 1 \end{bmatrix}. \tag{3.27}$$

Under the choice of D_s, the sliding variables $\sigma_2, \sigma_3,$ and σ_4 will couple to each other. As a result, the required control effort of T_{rl} also be provided by T_f and T_{rr} to compensate the degradation effect. A same scenario for state response can also be observed form Figs. 3.6(a)-(d). However, from Figs. 3.7(a)-(c), the slip ratios of these three wheel are slight variation because the couple effect of sliding variable. Fig. 3.8 shows the couple effect for $D_sB\sigma_2, D_sB\sigma_3,$ and $D_sB\sigma_4$. Fig 3.9 shows the control efforts. Among these, the control curves of T_f, T_{rr}, T_{rl} are slight different to pervious simulation result.

Although the combined scheme requires a little more control effort than SDRE1, it enables a much smaller yaw rate and lateral velocity than the SDRE1 scheme. Thus, it is concluded from this example that the combined scheme is more robust and safer in braking control than the SDRE scheme alone.

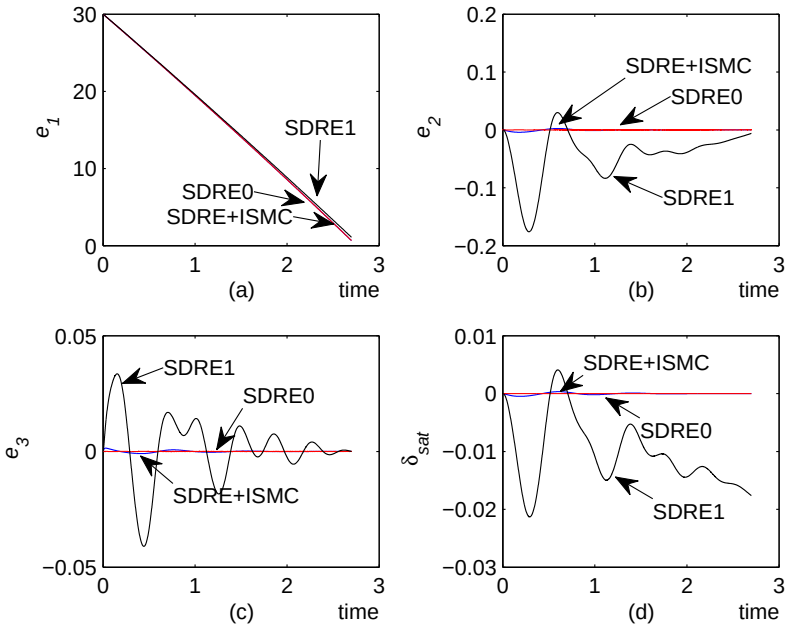

Fig. 3.2. Time history of the first four system states.

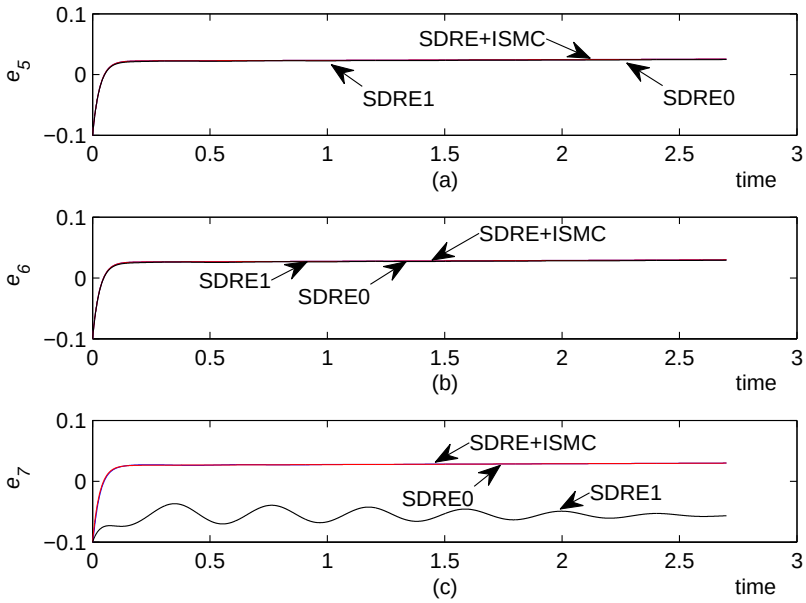

Fig. 3.3. Time history of the last three system states.

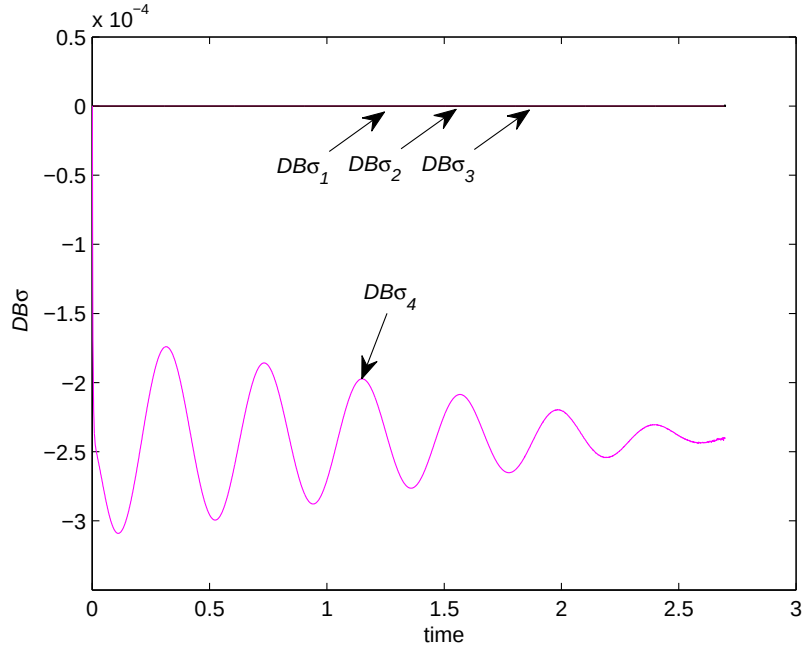

Fig. 3.4. Time history of the four sliding variables for SDRE+ISMC scheme.

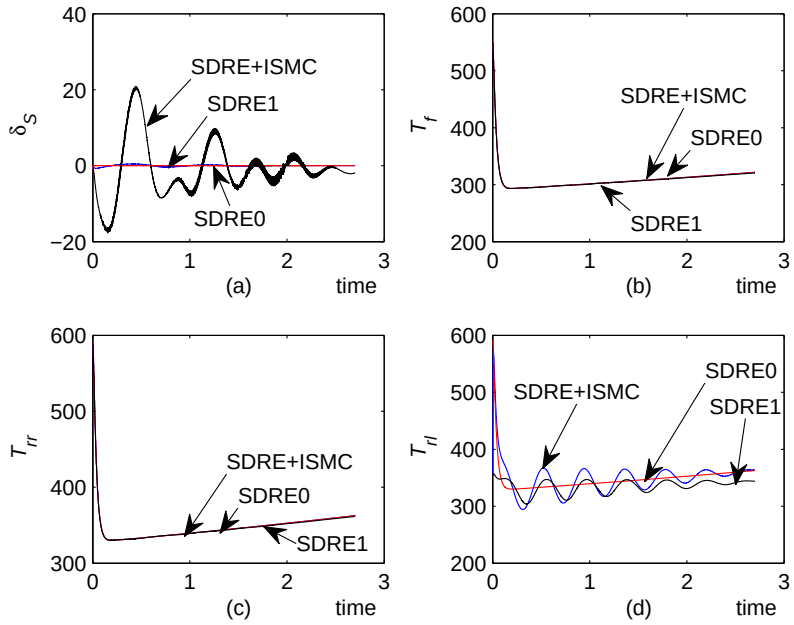

Fig. 3.5. Time history of the four control inputs.

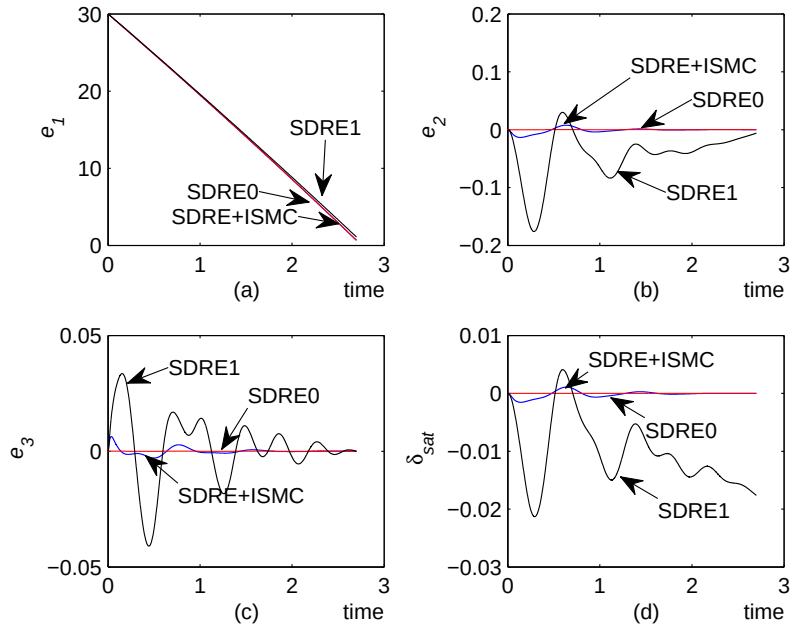

Fig. 3.6. Time history of the first four system states.

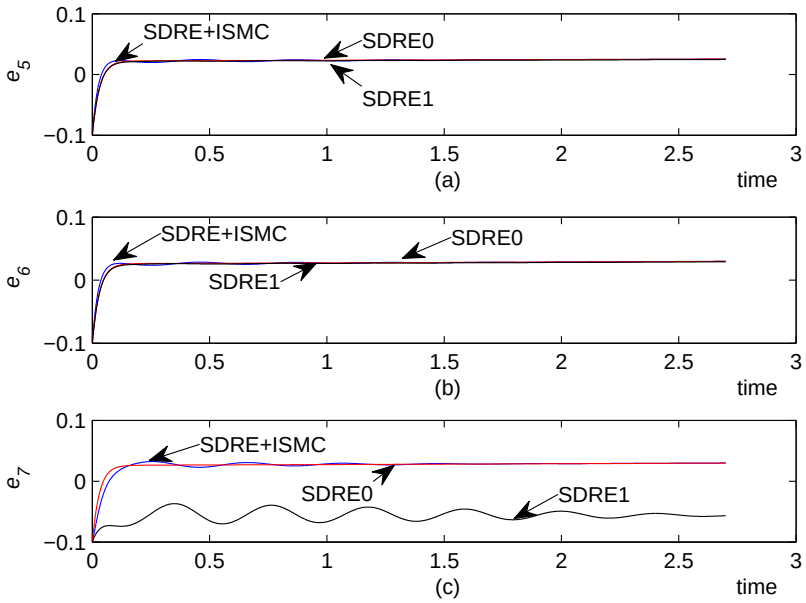

Fig. 3.7. Time history of the last three system states.

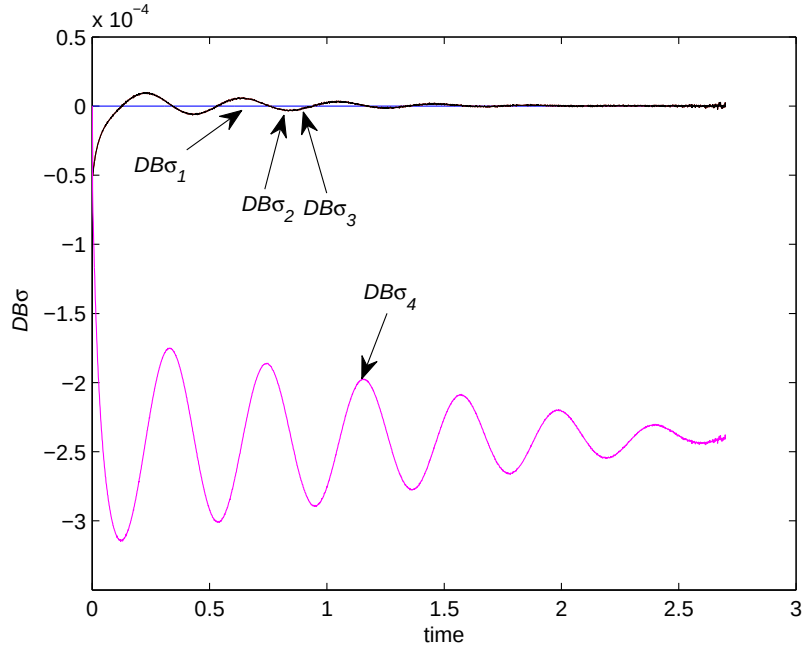

Fig. 3.8. Time history of the four sliding variables for SDRE+ISMC scheme.

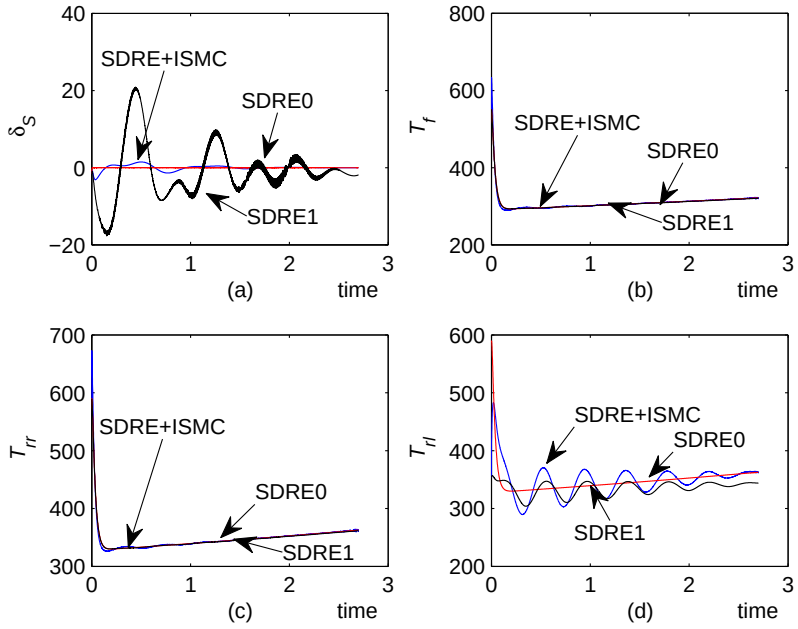

Fig. 3.9. Time history of the four control inputs.

Appendix 3.A

Here, we present $A_1(\mathbf{e}_1)$, $\mathbf{b}(\mathbf{e}_1)$ and $G_1(\mathbf{e}_1)$ for the TWV, which appear inside Eq. (3.6):

(i) Let $A_1(\mathbf{e}_1) = [a_{ij}]$. Then $a_{i1} = a_{4j} = a_{2k} = 0$ for $i = 1, \cdots, 7$, $j = 1, 2, 3, 5, 6, 7$, $k = 6, 7$ and

$$a_{12} = \frac{C_f s\delta_{sat}}{me_1};\ a_{13} = \frac{C_f l_1 s\delta_{sat}}{me_1} + e_2;\ a_{14} = \frac{-\delta_{sat} C_f s\delta_{sat}}{me_4}; a_{15} = \frac{-E_1 c\delta_{sat}}{m};\ a_{16} = \frac{-E_2}{m};$$

$$a_{17} = \frac{-E_3}{m}; a_{22} = \frac{-1}{m}\left(\frac{C_f c\delta_{sat}}{e_1} + \frac{C_{rr}}{e_1 - l_3 e_3} + \frac{C_{rl}}{e_1 + l_3 e_3}\right);$$

$$a_{23} = \frac{1}{m}\left(\frac{-C_f l_1 c\delta_{sat}}{e_1} + \frac{C_{rr} l_2}{e_1 - l_3 e_3} + \frac{C_{rl} l_2}{e_1 + l_3 e_3}\right) - e_1;\ a_{24} = \frac{\delta_{sat} \cdot C_f c\delta_{sat}}{me_4};\ a_{25} = \frac{-E_1 s\delta_{sat}}{m};$$

$$a_{32} = \frac{1}{J_v}\left(\frac{-C_f l_1 c\delta_{sat}}{e_1} + \frac{C_{rr} l_2}{e_1 - l_3 e_3} + \frac{C_{rl} l_2}{e_1 + l_3 e_3}\right);$$

$$a_{33} = \frac{-1}{I_{zz}}\left(\frac{C_f l_1^2 c\delta_{sat}}{e_1} + \frac{C_{rr} l_2^2}{e_1 - l_3 e_3} + \frac{C_{rl} l_2^2}{e_1 + l_3 e_3}\right);$$

$$a_{34} = \frac{\delta_{sat} \cdot l_1 C_f c\delta_{sat}}{J_v e_4};\ a_{35} = \frac{-l_1 E_1 s\delta_{sat}}{J_v};\ a_{36} = \frac{l_3 E_2}{I_{zz}};\ a_{37} = \frac{-l_3 E_3}{J_v};\ a_{44} = \frac{-1}{\tau};$$

$$a_{i2} = \frac{1 - e_i - \lambda_\alpha^*}{me_1} \cdot \frac{C_f s\delta_{sat}}{e_1} \text{ for } i = 5, 6, 7, \text{ and}$$

$\alpha = f, rr$ and rl if $i = 5, 6$ and 7, respectively;

$$a_{i3} = \frac{1-e_i-\lambda_\alpha^*}{me_1}\left(\frac{C_f l_1 s\delta_{sat}}{e_1}+e_2\right) \text{ for } i=5,6,7, \text{ and}$$
$$\alpha = f, rr \text{ and } rl \text{ if } i=5,6 \text{ and } 7, \text{ respectively;}$$
$$a_{i4} = -\frac{1-e_i-\lambda_\alpha^*}{me_1}\cdot\frac{\delta_{sat}\cdot C_f s\delta_{sat}}{e_4} \text{ for } i=5,6,7, \text{ and}$$
$$\alpha = f, rr \text{ and } rl \text{ if } i=5,6 \text{ and } 7, \text{ respectively;}$$
$$a_{55} = -\frac{1-e_5-\lambda_f^*}{me_1}\left(E_1 c\delta_{sat}+\frac{R_w^2}{J_w}E_1\right);$$
$$a_{i5} = -\frac{1-e_i-\lambda_\alpha^*}{me_1}\cdot E_1 c\delta_{sat} \text{ for } i=6,7, \text{ and}$$
$$\alpha = rr \text{ and } rl \text{ if } i=6 \text{ and } 7, \text{ respectively;}$$
$$a_{66} = -\frac{1-e_6-\lambda_{rr}^*}{me_1}\left(E_2+\frac{R_w^2}{J_w}E_2\right);$$
$$a_{i6} = -\frac{(1-e_i-\lambda_\alpha^*)E_2}{me_1} \text{ for } i=5,7, \text{ and}$$
$$\alpha = f \text{ and } rl \text{ if } i=5 \text{ and } 7, \text{ respectively;}$$
$$a_{77} = -\frac{1-e_7-\lambda_{rl}^*}{me_1}\left(E_3+\frac{R_w^2}{J_w}E_3\right);$$
$$a_{i7} = -\frac{(1-e_i-\lambda_\alpha^*)E_3}{me_1} \text{ for } i=5,6, \text{ and}$$
$$\alpha = f \text{ and } rr \text{ if } i=5 \text{ and } 6, \text{ respectively;}$$
$$E_i = -N_\alpha c_3 e^{-c_4(\lambda_\alpha^*+e_{i+4})e_1} \text{ for } i=1,2,3, \text{ and}$$
$$\alpha = f, rr \text{ and } rl \text{ if } i=1,2 \text{ and } 3, \text{ respectively.}$$

(ii) Let $\mathbf{b}(\mathbf{e}_1) = [b_1, \cdots, b_7]^T$. Then

$$b_1 = -\frac{E_5 c\delta_{sat}+E_6+E_7}{m};\ b_2 = \frac{-E_5 s\delta_{sat}}{m}; b_3 = \frac{1}{J_v}\left(-l_1 E_5 s\delta_{sat}+l_3 E_6 - l_3 E_7\right);\ b_4 = 0;$$
$$b_i = \frac{e_i+\lambda_\alpha^*-1}{me_1}\left(E_5 c\delta_{sat}+E_6+E_7+\frac{R_w^2}{J_w}E_i\right) \text{ for } i=5,6,7;$$
$$E_i = N_\alpha c_1 e^{-c_4(\lambda_\alpha^*+e_i)e_1}\left(1-e^{-c_2(\lambda_\alpha^*+e_i)}\right) - \lambda_\alpha^* N_\alpha c_3 e^{-c_4(\lambda_\alpha^*+e_i)e_1} \text{ for } i=5,6,7, \text{ and}$$
$$\alpha = f, rr \text{ and } rl \text{ if } i=5,6 \text{ and } 7, \text{ respectively.}$$

(iii) Let $G_1(\mathbf{e}_1) = [g_{ij}]$. Then $g_{ij} = 0$ for all i, j except for $g_{41} = \frac{1}{\tau}$ and $g_{52} = g_{63} = g_{74} = \frac{R_w}{e_1 J_w}$.

CHAPTER FOUR
A STUDY OF RELIABLE YAW MOMENT CONTROL FOR ELECTRIC VEHICLE

In this chapter, the SMC reliable control scheme is applied to retain steerability and lead the vehicle to a neutral steer behavior. This chapter is organized as follows. Section 4.1 states the vehicle dynamical model and the problem. It is followed by the design of SMC reliable controllers for ensuring EVs' safety when actuators' fault happens. Section 4.4 demonstrates the simulation results.

4.1 Problem Formulation

Consider the following 7 DOF nonlinear vehicle model [16]:

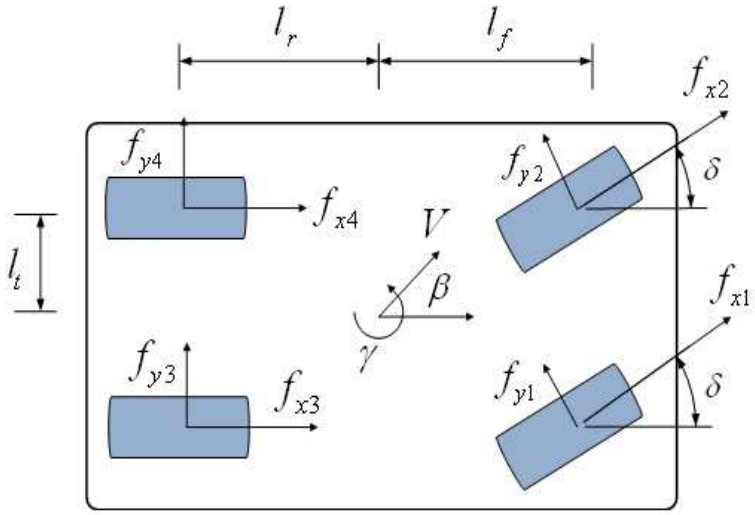

Fig. 4.1. Four wheeled vehicle model.

$$\begin{pmatrix} m\dot{V} \\ mV\dot{\beta} \\ J_v\dot{\gamma} \end{pmatrix} = \begin{pmatrix} 0 \\ -mV\gamma \\ 0 \end{pmatrix} + \begin{pmatrix} c\beta & s\beta & 0 \\ -s\beta & c\beta & 0 \\ 0 & 0 & 1 \end{pmatrix} \cdot \sum_{i=1}^{4} \begin{pmatrix} f_{x_i}c\delta_i - f_{y_i}s\delta_i \\ f_{x_i}s\delta_i + f_{y_i}c\delta_i \\ M_{z_i} \end{pmatrix} \tag{4.1}$$

$$\dot{\omega}_i = \frac{R_w f_{x_i} - T_i}{J_w} \tag{4.2}$$

$$\text{and } M_{z_i} = l_{x_i}(f_{x_i} c\delta_i - f_{y_i} s\delta_i) + l_{y_i}(f_{x_i} s\delta_i + f_{y_i} c\delta_i) \tag{4.3}$$

for $i = 1, \cdots, 4$. Here, c and s denote respectively the cosine and the sine functions (e.g., $c\beta = \cos\beta$ and $s\delta_i = \sin\delta_i$), m, J_v, J_w and R_w denote respectively the vehicle mass, vehicle inertia, wheel inertia and wheel radius, V, β and γ are respectively the vehicle velocity, body side slip angle and yaw rate, ω_i, δ_i and T_i for $i = 1, \cdots, 4$ denote respectively the wheel angular speed, steering wheel angle and brake/drive torque at the ith wheel, f_{x_i} and f_{y_i} denote the longitudinal and the lateral forces at the ith wheel between the tire patch and the road, respectively, and l_{x_i} and l_{y_i} denote respectively the lateral and longitudinal distances between the center of gravity (CG) to the ith wheel. In this chapter, the subscripts $i = 1, \cdots, 4$ are employed to represent respectively the front-right, the front-left, the rear-right and the rear-left wheels, as seen from the driver. Besides, we assume that $\delta_1 = \delta_2 = \delta$, $\delta_3 = \delta_4 = 0$, $l_{x1} = l_{x3} = -l_t$, $l_{x2} = l_{x4} = l_t$, $l_{y1} = l_{y2} = l_f$ and $l_{y3} = l_{y4} = -l_r$ [16]. The longitudinal and the lateral forces are expressed according to the Magic Formula [37] as follows:

$$f_{x_i}(\lambda_i) = D \sin\left\{C \tan^{-1}\left[B\lambda_i - E\left(B\lambda_i - \tan^{-1}(B\lambda_i)\right)\right]\right\} \tag{4.4}$$

$$\text{and } f_{y_i}(\alpha_i) = D \sin\left\{C \tan^{-1}\left[B\alpha_i - E\left(B\alpha_i - \tan^{-1}(B\alpha_i)\right)\right]\right\} \tag{4.5}$$

for $i = 1, \cdots, 4$, where the coefficients B, C, D and E denote respectively the stiffness, the shape, the peak, and the curvature factors, λ_i and α_i are respectively the wheel slip ratio and the tire slip angle defined by [16] as

$$\lambda_i = \frac{(V - R_w\omega_i)}{\max\{V, R_w\omega_i\}}, \ i = 1, \cdots, 4 \tag{4.6}$$

$$\text{and } \alpha_i = \begin{cases} -\tan^{-1}\left(\frac{l_f\gamma + Vs\beta}{Vc\beta}\right) + \delta, & i = 1, 2 \\ \tan^{-1}\left(\frac{l_r\gamma - Vs\beta}{Vc\beta}\right), & i = 3, 4. \end{cases} \tag{4.7}$$

Note that, $\lambda_i < 0$ if the ith wheel is in acceleration, and $\lambda_i > 0$ if it is in deceleration.

In order to have a satisfactory steerability and guide the vehicle to a neutral steer behavior, a reference yaw rate γ_d determined from the assumption of constant forward

speed, while negotiating a steady state cornering maneuver has been proposed as (4.8)-(4.9) below [4]:

$$\gamma_d = \frac{\gamma_{ss}}{1+\tau p}\delta \tag{4.8}$$

$$\text{and } \gamma_{ss} = \frac{2VC_fC_r\left(l_f+l_r\right)}{2C_fC_r\left(l_f+l_r\right)^2 - mV^2\left(l_fC_f - l_rC_r\right)} \tag{4.9}$$

where τ, p, C_f and C_r denote the time constant, the Laplace variable, the front and the rear wheel cornering stiffness, respectively. When the vehicle is operated under normal (non-faulty) condition, the desired yaw rate can be easily tracked by creating a yaw moment from the difference of tire driving torques and/or braking forces between the right and left sides. However, if one of the wheel torque controllers fails to operate (which might result from the inverter failure, the brake system failure, or the wheel motor failure [41]), the vehicle will start to spin and an appropriate reliable controller is needed to assure driving safety and provide better performances. Thus, the objective of this chapter is to organize a suitably control to realize the performance $\gamma \to \gamma_d$ when a vehicle experiences wheel actuator failure.

4.2 Reliable Controller Design

4.2.1 Output tracking formulation

Let $\mathbf{x} = [V, \beta, \gamma, \omega_1, \omega_2, \omega_3, \omega_4]$, $\mathbf{u} = [T_1, T_2, T_3, T_4]$ and $y = \gamma$. Then Eqs. (4.1)-(4.2) together with the selected output γ constitute a multi-input and single-output (MISO) nonlinear affine system. It is found that the MISO system has relative degree 2, i.e., one has to differentiate $y(t)$ twice to have $\mathbf{u}(t)$ explicitly appearing. By direct calculation we have

$$\ddot{\gamma} = \phi\left(\mathbf{x}\right) + G\left(\mathbf{x}\right)\mathbf{u} + d \tag{4.10}$$

where $\phi(\mathbf{x}) \in \mathbb{R}$, $G(\mathbf{x}) = [g_1(\mathbf{x}), \cdots, g_4(\mathbf{x})] \in \mathbb{R}^4$, d denotes possible uncertainties and/or measurement noises, and the detailed expressions of $\phi(\mathbf{x})$ and $g_i(\mathbf{x})$ are given as below: Define

$$\varpi_1(x) = Bx - E\left[Bx - \tan^{-1}(Bx)\right] \tag{4.11}$$

$$\varpi_2(x) = C\tan^{-1}\left[\varpi_1(x)\right] \tag{4.12}$$

$$\varpi_3(x) \;=\; \frac{BCD\cos(\varpi_2(x))[(1-E)(1+B^2x^2)+E]}{(1+\varpi_1^2(x))(1+B^2x^2)}. \tag{4.13}$$

Then $f_{x_i}(\lambda_i) = D\sin(\varpi_2(\lambda_i))$, $f_{y_i}(\alpha_i) = D\sin(\varpi_2(\alpha_i))$, $\frac{d}{dt}f_{x_i}(\lambda_i) = \varpi_3(\lambda_i)\dot{\lambda}_i$ and $\frac{d}{dt}f_{y_i}(\alpha_i) = \varpi_3(\alpha_i)\dot{\alpha}_i$. These together with Eqs. (4.1)-(4.3) and (4.6)-(4.7) yield

$$\begin{aligned}\phi(\mathbf{x}) \;=\; \frac{1}{J_v}\sum_{i=1}^{4}\Big\{ &-l_{x_i}\left(f_{x_i}s\delta_i + f_{y_i}c\delta_i\right)\dot{\delta}_i + l_{y_i}\left(f_{x_i}c\delta_i - f_{y_i}s\delta_i\right)\dot{\delta}_i \\ &+(l_{x_i}c\delta_i + l_{y_i}s\delta_i)\varpi_3(\lambda_i)\dot{\lambda}_{xi} + (l_{y_i}c\delta_i - l_{x_i}s\delta_i)\varpi_3(\alpha_i)\dot{\alpha}_i\Big\} \end{aligned} \tag{4.14}$$

$$\text{and } g_i(\mathbf{x}) \;=\; \frac{1}{J_v}\left(l_{x_i}c\delta_i + l_{y_i}s\delta_i\right)\varpi_3(\lambda_i)\dot{\lambda}_{ui} \tag{4.15}$$

for $i = 1, \cdots, 4$, where

$$\dot{\lambda}_{xi} = \begin{cases} \frac{J_wR_w\omega_i\dot{V} - R_w^2Vf_{x_i}}{J_wV^2} & \text{if } \lambda_i > 0 \\ \frac{\dot{V}}{R_w\omega_i} - \frac{Vf_{x_i}}{J_w\omega_i^2} & \text{if } \lambda_i < 0 \end{cases} \tag{4.16}$$

$$\dot{\lambda}_{ui} = \begin{cases} \frac{R_w}{J_wV} & \text{if } \lambda_i > 0 \\ \frac{V}{J_wR_w\omega_i^2} & \text{if } \lambda_i < 0 \end{cases} \tag{4.17}$$

$$\dot{\alpha}_i = \begin{cases} \dot{\delta} - \frac{(V^2 - l_f\gamma Vs\beta)\dot{\beta} + l_fVc\beta\dot{\gamma} - l_f\gamma c\beta\dot{V}}{(Vc\beta)^2 + (l_f\gamma + Vs\beta)^2} & \text{if } i = 1, 2 \\ \frac{(l_r\gamma Vs\beta - V^2)\dot{\beta} + l_rVc\beta\dot{\gamma} - l_r\gamma c\beta\dot{V}}{(Vc\beta)^2 + (l_r\gamma - Vs\beta)^2} & \text{if } i = 3, 4. \end{cases} \tag{4.18}$$

4.2.2 SMC reliable design

In this chapter we consider the active reliable output tracking issues for System (4.1)-(4.2), that is, we assume that the actuators' fault has been successfully detected and diagnosed by an FDD mechanism. The fault may be time varying and include degradation, amplification and outage [28]. Before the occurrence of faults, the engineers may take any kind of control strategy to fulfill their desired system performance. When the fault is detected and diagnosed, the control law is guided to switch to an active reliable law for ensuring system performance. Thus, after the fault is detected, we may divide the actuators into two groups $\mathcal{H}$ and $\mathcal{F}$, within which we assume that all of the actuators in $\mathcal{H}$ are healthy, while those in $\mathcal{F}$ experience faults. This implies that Eq. (4.10) can be rewritten as

$$\ddot{\gamma} = \phi(\mathbf{x}) + G_{\mathcal{H}}(\mathbf{x})\,\mathbf{u}_{\mathcal{H}} + G_{\mathcal{F}}(\mathbf{x})\,\mathbf{u}_{\mathcal{F}} + d \tag{4.19}$$

where $\mathbf{u} = [\mathbf{u}_{\mathcal{H}}^T\ \mathbf{u}_{\mathcal{F}}^T]^T$ and $G(\mathbf{x}) = [G_{\mathcal{H}}(\mathbf{x})\ G_{\mathcal{F}}(\mathbf{x})]$. In the rest of the this paper, we assume that $\mathbf{u}_{\mathcal{H}} \in \mathbb{R}^{\mathrm{k}}$, $\mathbf{u}_{\mathcal{F}} \in \mathbb{R}^{4-\mathrm{k}}$ and $k \geq 1$, since the assumption of $\mathrm{rank}(G_{\mathcal{H}}(\mathbf{x})) = 1$ is

necessary for the existence of the equivalent control in SMC design [9]. In addition, we assume that the control inputs in the set of $\mathcal{F}$ are diagnosed as

$$\mathbf{u}_{\mathcal{F}} = \hat{\mathbf{u}}_{\mathcal{F}} + \Delta\mathbf{u}_{\mathcal{F}} \tag{4.20}$$

where $\hat{\mathbf{u}}_{\mathcal{F}}$ and $\Delta\mathbf{u}_{\mathcal{F}}$ denote the estimated control value and estimated error, respectively. The estimated error $\Delta\mathbf{u}_{\mathcal{F}}$ is treated as an additional uncertainty that should be compensated. Define the output error

$$e = \gamma - \gamma_d. \tag{4.21}$$

The control objective is then to force $e \to 0$ through SMC reliable design. Since Eq. (4.19) is a second-order system, we may assume the sliding surface in the form of

$$\sigma = \dot{e} + k_2 e \tag{4.22}$$

where k_2 is a positive constant. Clearly, if the system state remains on the sliding surface, then the desired performance of $e \to 0$ can be exponentially achieved with a convergence rate depending on the choice of k_2 [9]. From Eqs. (4.19)-(4.22) we have

$$\dot{\sigma} = \phi(\mathbf{x}) + G_{\mathcal{H}}\mathbf{u}_{\mathcal{H}} + G_{\mathcal{F}}\left(\hat{\mathbf{u}}_{\mathcal{F}} + \Delta\mathbf{u}_{\mathcal{F}}\right) + d - \ddot{\gamma}_d + k_2\dot{e}. \tag{4.23}$$

To guarantee the reaching performance, we impose the next assumption:

Assumption 4.1: There exists a nonnegative function $\rho(\mathbf{x}, t)$ such that $|G_{\mathcal{F}}\Delta\mathbf{u}_{\mathcal{F}} + d| \leq \rho(\mathbf{x}, t)$.

Following the SMC design procedure [9], we choose

$$\begin{aligned} \mathbf{u}_{\mathcal{H}} \;=\; & -G_{\mathcal{H}}^{+}(\mathbf{x}) \cdot [\phi(\mathbf{x}) + G_{\mathcal{F}}(\mathbf{x})\,\hat{\mathbf{u}}_{\mathcal{F}} - \ddot{\gamma}_d + k_2\dot{e} \\ & + (\rho(\mathbf{x}, t) + \eta)\,\mathrm{sgn}(\sigma)] \end{aligned} \tag{4.24}$$

where $G_{\mathcal{H}}^{+}(\mathbf{x}) = G_{\mathcal{H}}^{T}(\mathbf{x})\left[G_{\mathcal{H}}(\mathbf{x})\;\; G_{\mathcal{H}}^{T}(\mathbf{x})\right]^{-1}$ and η is a positive constant which affects the convergence speed of the system state to the sliding surface. Note that, $\mathbf{u}_{\mathcal{H}}$, given by (4.24), involves the information of diagnosis. Form (4.23), (4.24) and Assumption 1 we have

$$\begin{aligned} \sigma\dot{\sigma} \;&=\; \sigma \cdot [G_{\mathcal{F}}\Delta\mathbf{u}_{\mathcal{F}} + d - (\rho(\mathbf{x}, t) + \eta)\,\mathrm{sgn}(\sigma)] \\ &\leq\; -\eta|\sigma|. \end{aligned} \tag{4.25}$$

Thus, the system state will reach the sliding surface in a finite amount of time with reaching speed depending on the magnitude of η, and remain there hereafter [9]. After reaching to the sliding surface $\sigma = 0$, the tracking error e, from Eq. (4.22), satisfies $\dot{e} + ke = 0$. It implies that the tracking error is exponentially convergent to zero and the tracking performance is achieved. In addition to the yaw rate tracking, another factor that affects the vehicle driving stability and cannot be ignored is the magnitude of the body side slip angle β. It is in general expected to have β as small as possible for ensuring vehicle stability; however, when $\gamma \approx \gamma_d$, $|\dot{V}| \approx 0$, $|\beta| \ll 1$, $l_t\gamma_d/V \ll 1$ and the tire forces at the two sides are the same, the side slip angle is related to the yaw rate and the steering angle in the following relation [40]:

$$\begin{aligned}\dot{\beta} \approx & -\left(\frac{2C_f + 2C_r}{mV}\right)\beta + \left(\frac{2C_r l_r - 2C_f l_f}{mV^2} - 1\right)\gamma_d \\ & + \left(\frac{2C_f + 2C_r}{mV}\right)\delta \end{aligned} \tag{4.26}$$

which is clearly a stable system for β with inputs γ_d and δ. As a result, the side slip angle is determined from the yaw rate and the steering angle, and it can be made small if γ_d and δ are appropriately chosen. An analysis of lateral stability and bifurcation phenomena with respect to the variations in the front wheel steering angle has been presented in [29]. Besides, one may also deal with the tracking of yaw rate and side slip angle simultaneously by choosing the weightings on the error of yaw rate and on the error of side slip angle [11]. In this chapter, we only consider the yaw rate tracking matter, i.e., the weighting on the error of side slip angle is chosen to be zero.

4.2.3 FDD mechanism

To detect the actuators' fault for active reliable task, in this chapter we assume that all the state variables are available for measurement or estimation. In fact, this assumption is feasible for EVs [4]. We adopt the observer and the associated residual signals r_i from [22] as (4.27 and (4.28) below:

$$\dot{\zeta}_i = \frac{R_w f_{x_i} - T_i}{J_w} + a_i\left(\omega_i - \zeta_i\right) \tag{4.27}$$

$$\text{and } r_i = \omega_i - \zeta_i \tag{4.28}$$

where $i = 1, \cdots, 4$ and $a_i > 0$ for all i. It was shown in [22] that the actuators' fault can be detected and diagnosed with diagnosed error converging to zero at an exponential rate a_i.

4.3 Simulation Results

In this chapter, we adopt the vehicle's parameters from [38] as follows: $m = 1300$kg, $J_v = 2000$kgm^2, $J_w = 0.6$kgm^2, $l_f = 1.25$m, $l_r = 1.25$m, $l_t = 0.8$m and $R_w = 0.3$m. Under these settings, the normal loads for the four wheels are calculated to be $F_{z_i} = mgl_r/2l = 3188$N for $i = 1, 2$ and $F_{z_i} = mgl_f/2l = 3188$N for $i = 3, 4$. Let the cornering stiffness $C_f = C_r = 8741$N/rad. The coefficients of the Magic Formula can then be obtained as follows: $B = 0.1664$, $C = 1.65$, $D = 3579.4$ and $E = 0.6645$ for longitudinal forces; and $B = 0.2302$, $C = 1.3$, $D = 3152.9$ and $E = -0.0412$ for lateral forces [37]. The control and the observer parameters are selected as $\tau = 10^{-3}$, $k_2 = 1$, $\eta = 1$ and $a_i = 1$ for $i = 1, \cdots, 4$. To alleviate chatter, $\text{sgn}(\sigma)$ is replaced with the saturation function $\text{sat}(\sigma/\epsilon)$ and $\epsilon = 10^{-1}$. The steering command for lane change is chosen to be $\delta = 0.05 \sin(1.5708(t-1))$ when $1 \leq t \leq 5$, and $\delta = 0$ elsewhere [4]. Finally, the road is assumed to be dry, and the initial state and the disturbance are taken as $\mathbf{x}(0) = [30, 0, 0.5, 10^2, 10^2, 10^2, 10^2]$ and $d = \sin(20t) + 0.5\sin(30t) + 0.1\sin(50t)$.

To demonstrate the reliable performances, in the following, we will consider three faulty cases: the first concerns only one actuator fault, two actuator faults and three actuators fault. The alarm will be fired if any one of the residual signals exceeds 1 (i.e., $|r_i| > 1$). Numerical results are summarized in Figs. 4.2-4.13. Among these, we adopt the following two schemes: the first uses the proposed reliable SMC scheme (labeled RSMC), while the other adopts the conventional (non-reliable) SMC design (labeled SMC). Before alarm, both the two schemes adopt their conventional non-reliable SMC design, i.e., control in the form of (4.24) with all actuators being healthy. Whenever there is an alarm, the associate active reliable controllers are activated according to the FDD information.

4.3.1 One actuator fault

Here, we assume that the rear-left brake actuator fails at $t = 2.5$, i.e., $T_4 = 0$ after $t = 2.5$, $\mathcal{H} = \{T_1, T_2, T_3\}$ and $\mathcal{F} = \{T_4\}$ after the fault happens. It is observed from Figs. 1(c) and 1(d) that the output tracking error for RSMC is much smaller than that of SMC after fault happens. The longitudinal velocity, as seen from Fig. 4.2(a), of RSMC decreases from 30m/sec to 24.48m/sec, while that of SMC decreases from 30m/sec to 16.3m/sec. This means that the non-reliable design leads to a larger deceleration than the RSMC; however, a large deceleration usually results in a loss of ride comfort [4], which is usually undesired. From Fig. 4.2(b), the magnitude of the side slip angle of RSMC is also significantly reduced after fault happens, compared with that of SMC. With the selected parameters and steering command, it is found that $\max\{l_t\gamma_d/V\}|_{V=30} = 0.016$ and Eq. (4.26) under $V \equiv 30$ becomes $\dot{\beta} = -0.90\beta - \gamma_d + 0.90\delta$, which yields the magnitude of β has an upper bound $\max_{t>0}|\beta| = 0.3678$ at around $t = 2.60$. It is observed from Fig. 4.2(b) that the magnitude of β for RSMC is actually within this bound. Besides, β of SMC is noticed from Fig. 4.2(b) to be convergent to zero slower than that of RSMC, because the output tracking error of SMC in Fig. 4.2(d) converges to zero slower than that of RSMC. Figures 4.3(a)-(d) show the angular speed of the four wheels. All of the four wheels are seen to be decelerated during the change lane period, and those of SMC having angular speed much decreased than those of RSMC. In addition, it is observed from Fig. 4.4(a) that the actuator fault is successfully detected by the observer at around $t = 2.506$. When the fault is detected, the RSMC scheme switches its controller to the reliable one and the residual signal r_4 is seen to quickly decrease to zero. This can also be seen from the alarm signals shown in Fig. 4.4(b), where the alarm value 1 denotes the fault of the fourth actuator. Figures 4.4(c) and 4.4(d) give the history of the four control torques for RSMC and SMC, respectively. It is noted that after the detection of the outage of actuator T_4, the other three actuators of RSMC contribute much more control effort than those of SMC to realize the required yaw moment for yaw rate tracking, which are also reflected in Figs. 4.2(b) and 4.2(d) where the output tracking performances of RSMC are much better than those of SMC. After the change lane mission (i.e., $t \geq 5$),

the controls of RSMC are seen from Fig. 4.4(c) to maintain near zero level, while those of SMC do not reduce to zero until the output tracking error converges to zero, as seen from Fig. 4.4(d). All the peaks of the healthy control curves and the abrupt change of $\gamma - \gamma_d$ at $t = 5$ of the SMC scheme come from the abrupt change of the steering wheel angle. Finally, Fig. 4 displays the time history of the sliding variables of RSMC and SMC. It is seen that, after the reaching phase time period, the two sliding variables remain inside the boundary layer before the fault happens. After the fault, the sliding variable of RSMC runs out of the boundary layer shortly and then gets back to the boundary layer due to the activation of reliable controller; however, the non-reliable scheme is not able to force its sliding variable stay inside the boundary layer even after the end of change lane mission $t \geq 5$. The two abrupt changes of σ of SMC scheme at $t = 3$ and $t = 5$ come from the occurrence of fault and control peak of SMC (see Fig. 4.4(d)), respectively. The final peak of the sliding variable curve of SMC near $t = 7$ is resulted from Eq. (4.22) and the abrupt change of $e = \gamma - \gamma_d$ shown in Fig. 4.2(d). These observations agree with the theoretical results.

4.3.2 Two actuator faults

In this section, we assume that the rear-left brake actuator fails at $t = 2.5$ and the front-right actuator fails at $t = 3$. That is, $T_4 = 0$ and $T_1 = 0$ after $t = 2.5$ and $t = 3$, respectively. These yield $\mathcal{H} = \{T_1, T_2, T_3\}$ and $\mathcal{F} = \{T_4\}$ during the time period $2.5 \leq t \leq 3$, and $\mathcal{H} = \{T_2, T_3\}$ and $\mathcal{F} = \{T_1, T_4\}$ after $t = 3$. It is observed from Figs. 4.6-4.7 that the timing responses of the seven states and the output tracking error for RSMC scheme have the same scenario as those of one fault case. However, from Figs. 4.2(a) and 4.6(a), the longitudinal velocity V of SMC scheme decreases from 30m/sec to 12.14m/sec, which is falling more than that of one fault case. The same scenarios can also be found from Figs. 4.3 and 4.7 regarding the four wheel angular velocities of SMC scheme. After the second fault, the side slip angle β and the output tracking error $\gamma - \gamma_d$ of the SMC scheme are seen to be a little larger than those of SMC regarding one fault case. From Fig. 4.8(a), the two actuator faults are observed to be successfully detected by the observer at around $t = 2.506$ and $t = 3.003$, respectively, which can also be seen

from the alarm signals shown in Fig. 4.8(b). When these faults are detected, the RSMC scheme switches its controller to the appropriately reliable one and the residual signals r_4 and r_1 are seen to quickly decrease to zero. Figures 4.8(c) and 4.8(d) give the time history of the four control torques for RSMC and SMC, respectively. It is noted that these control curves are exactly the same as those of one fault case before the second fault happens. After the detection of the second fault, the two healthy actuators T_2 and T_3 of RSMC contribute more control effort than one fault case and the SMC scheme to realize the required yaw moment for yaw rate tracking, as seen from Figs. 4.4(c), 4.8(c) and 4.8(d).

Finally, Fig. 4.9 displays the time history of the sliding variables of RSMC and SMC. Again, after the reaching phase time period, the two sliding variables remain inside the boundary layer before the first fault happens. When the two faults happen, the sliding variable of RSMC starts to grow and runs out of the boundary layer shortly, then it gets back to the boundary layer due to the activation of reliable controller. On the other hand, the non-reliable scheme is not able to force its sliding variable stay inside the boundary layer even after the end of change lane mission. The reasons for the abrupt changes of the $\sigma-$curve of SMC at $t = 2.5$ and $t = 5$, and the peak around $t \approx 7.8$ are same with those of one fault case. These observations agree with the theoretical results. From these examples, it is found that the performances of RSMC are better than those of conventional SMC design when the EVs experience actuators' faults.

4.3.3 Three actuator faults

In this section, we assume that the rear-left brake actuator fails at $t = 2.5$, the front-right actuator fails at $t = 3$, and the rear-right actuator fails at $t = 3.5$. That is, $T_4 = 0$, $T_1 = 0$ and $T_3 = 0$ after $t = 2.5$, $t = 3$ and $t = 3.5$, respectively. These yield $\mathcal{H} = \{T_1, T_2, T_3\}$ and $\mathcal{F} = \{T_4\}$ during the time period $2.5 \leq t \leq 3$, $\mathcal{H} = \{T_2, T_3\}$ and $\mathcal{F} = \{T_1, T_4\}$ during the time period $3 \leq t \leq 3.5$. $\mathcal{H} = \{T_2\}$ and $\mathcal{F} = \{T_1, T_3, T_4\}$ after $t = 3.5$. It is observed from Figs. 4.10-4.11 that the timing responses of the seven states and the output tracking error for RSMC scheme have the same scenario as those of one fault case. However, from Figs. 4.2(a), 4.6(a) and 4.10(a), the longitudinal velocity V

of SMC scheme decreases from 30m/sec to 11.15m/sec, which is falling more than those of one fault and two fault cases. The same scenarios can also be found from Figs. 4.3, 4.7 and 4.11 regarding the four wheel angular velocities of SMC scheme. After the three fault, the side slip angle β and the output tracking error $\gamma - \gamma_d$ of the SMC scheme are seen to be a little larger than those of SMC regarding one fault and two fault case. From Fig. 4.12(a), the three actuator faults are observed to be successfully detected by the observer at around $t = 2.506$, $t = 3.003$, and $t = 3.506$, respectively, which can also be seen from the alarm signals shown in Fig. 4.12(b). When these faults are detected, the RSMC scheme switches its controller to the appropriately reliable one and the residual signals r_4, r_1 and r_3 are seen to quickly decrease to zero. Figs. 4.12(c) and 4.12(d) give the time history of the four control torques for RSMC and SMC, respectively. It is noted that these control curves are exactly the same as those of one fault case before the second fault happens. After the detection of the third fault, the healthy actuator T_2 of RSMC contribute more control effort than one fault and two fault case. The SMC scheme realize the required yaw moment for yaw rate tracking, as seen from Figs. 4.4(c) 4.4(d), 4.8(c), 4.8(d), 4.12(c) and 4.12(d).

Finally, Fig. 4.13 displays the time history of the sliding variables of RSMC and SMC. Again, after the reaching phase time period, the two sliding variables remain inside the boundary layer before the first fault happens. When the two faults happen, the sliding variable of RSMC starts to grow and runs out of the boundary layer shortly, then it gets back to the boundary layer due to the activation of reliable controller. In addition, When the three faults happen, the sliding variable of RSMC starts to grow and runs out of the boundary layer shortly, then it gets back to the boundary layer due to the activation of reliable controller. On the other hand, the non-reliable scheme is not able to force its sliding variable stay inside the boundary layer even after the end of change lane mission. The reasons for the abrupt changes of the $\sigma-$curve of SMC at $t = 2.5$ and $t = 5$, and the peak around $t \approx 7.95$ are same with those of one fault and two fault case. These observations agree with the theoretical results. From these examples, it is found that the performances of RSMC are better than those of conventional SMC design when the EVs experience actuators' faults.

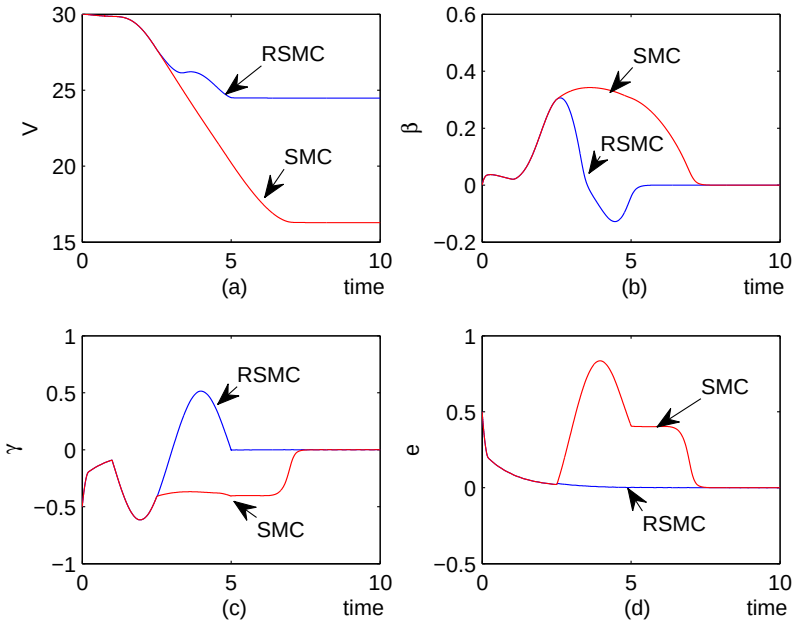

Fig. 4.2. Time histories of (a) longitudinal velocity, (b) body side slip angle, (c) yaw rate and (d) output tracking error for one actuator fault.

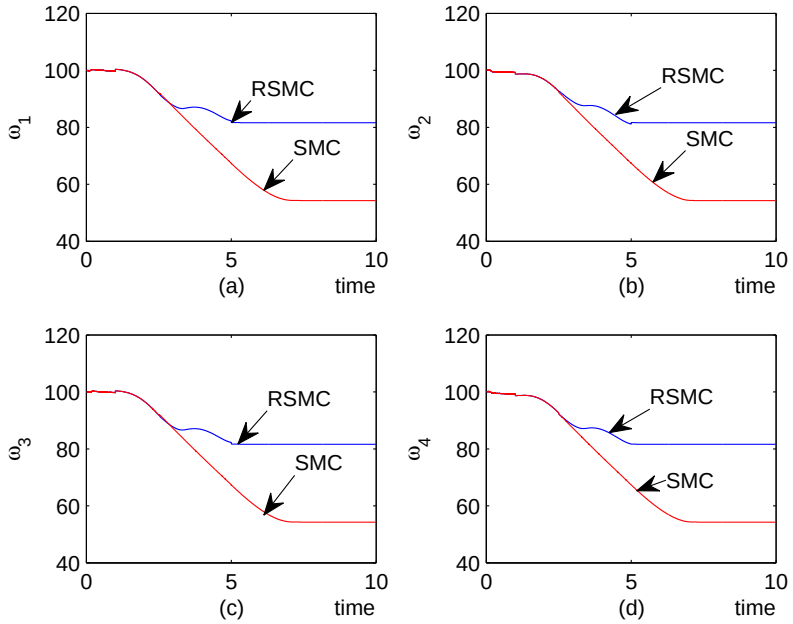

Fig. 4.3. Time histories of (a) front-right, (b) front-left, (c) rear-right and (d) rear-left wheel angular speeds for one actuator fault.

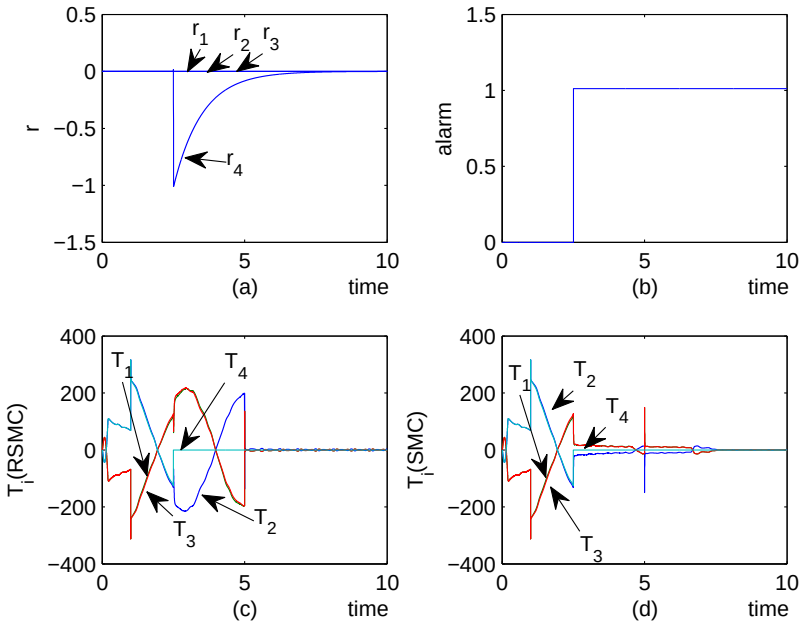

Fig. 4.4. (a) Residual signals; (b) alarm signal; (c) controls of RSMC and (d) Controls of SMC for one actuator fault.

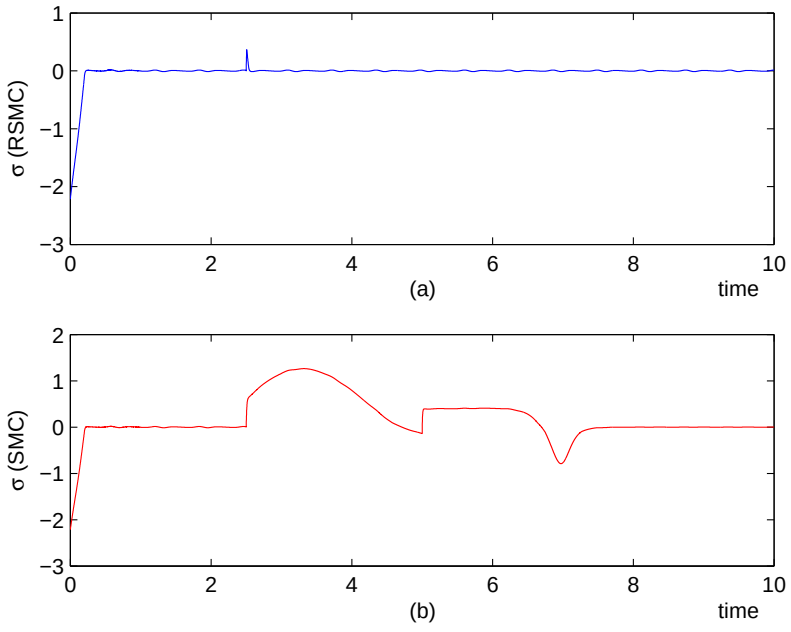

Fig. 4.5. Sliding variables of (a) RSMC and (b) SMC schemes for one actuator fault.

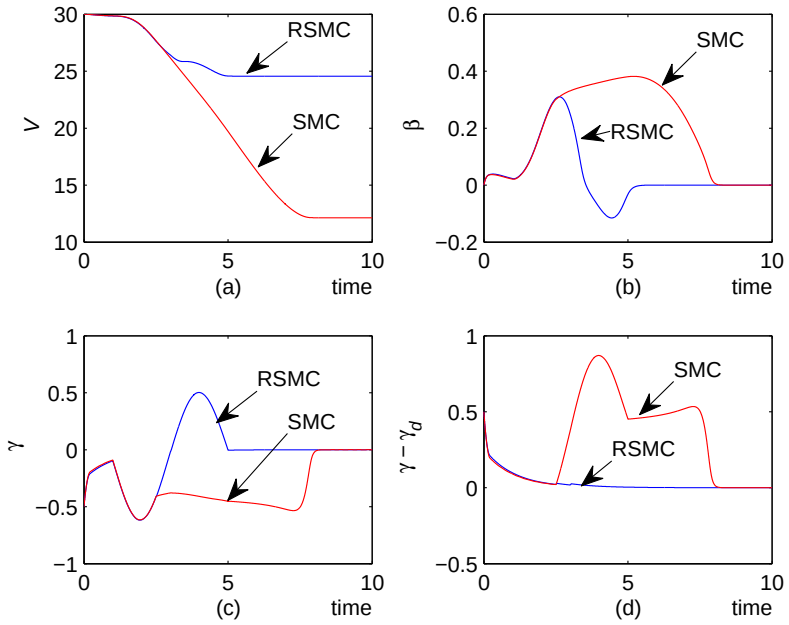

Fig. 4.6. Time histories of (a) longitudinal velocity, (b) body side slip angle, (c) yaw rate and (d) output tracking error for two actuator faults.

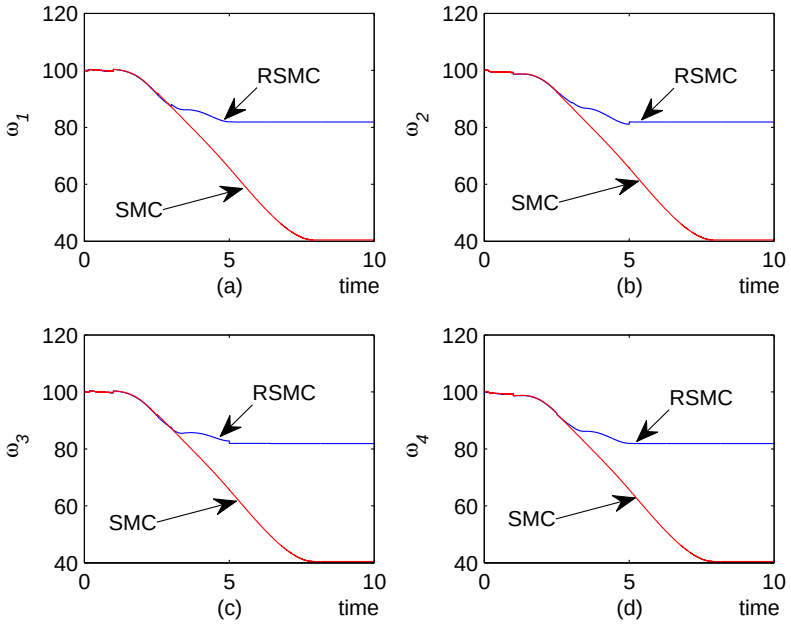

Fig. 4.7. Time histories of (a) front-right, (b) front-left, (c) rear-right and (d) rear-left wheel angular speeds for two actuator faults.

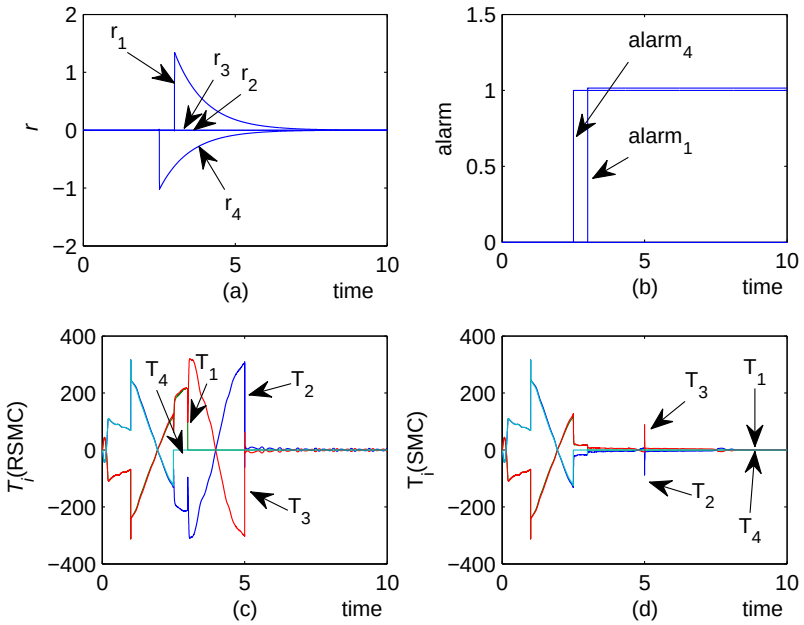

Fig. 4.8. (a) Residual signals; (b) alarm signal; (c) controls of RSMC and (d) Controls of SMC for two actuator faults.

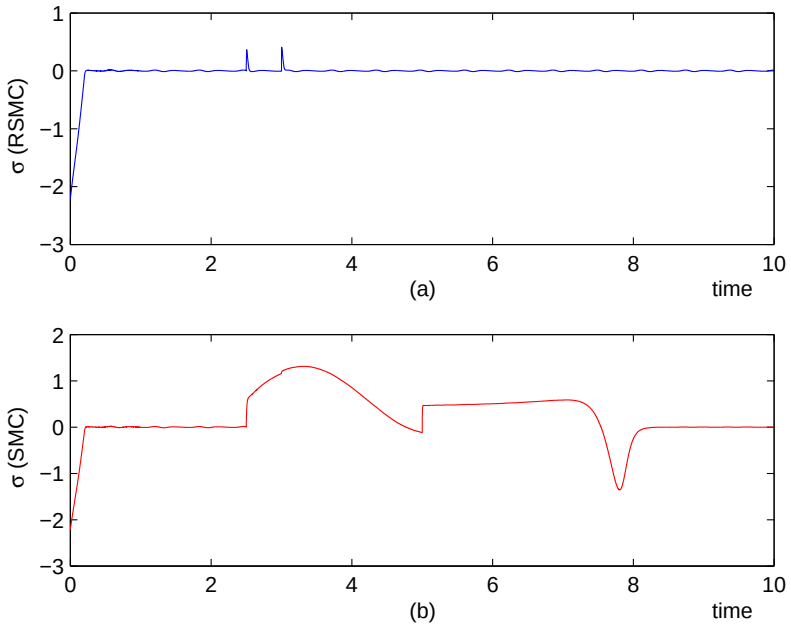

Fig. 4.9. Sliding variables of (a) RSMC and (b) SMC schemes for two actuator faults.

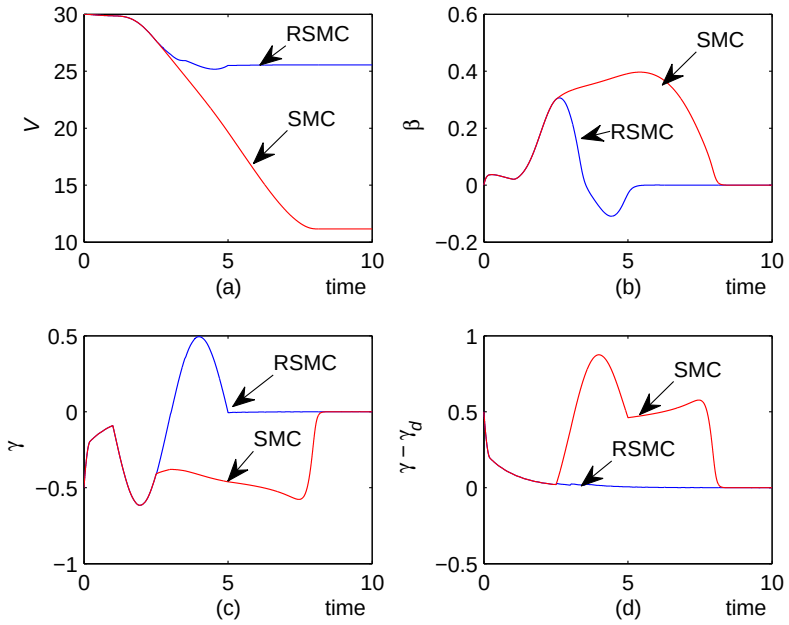

Fig. 4.10. Time histories of (a) longitudinal velocity, (b) body side slip angle, (c) yaw rate and (d) output tracking error for three actuator faults.

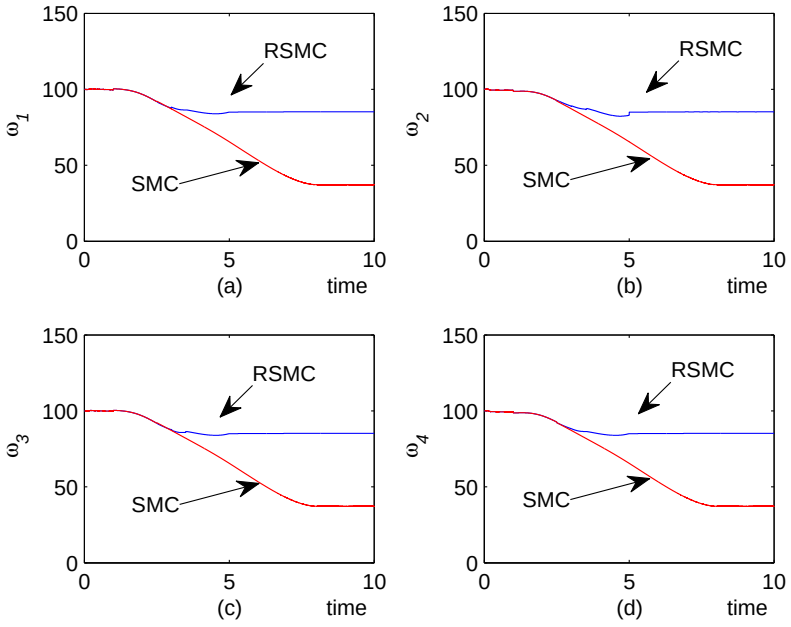

Fig. 4.11. Time histories of (a) front-right, (b) front-left, (c) rear-right and (d) rear-left wheel angular speeds for three actuator faults.

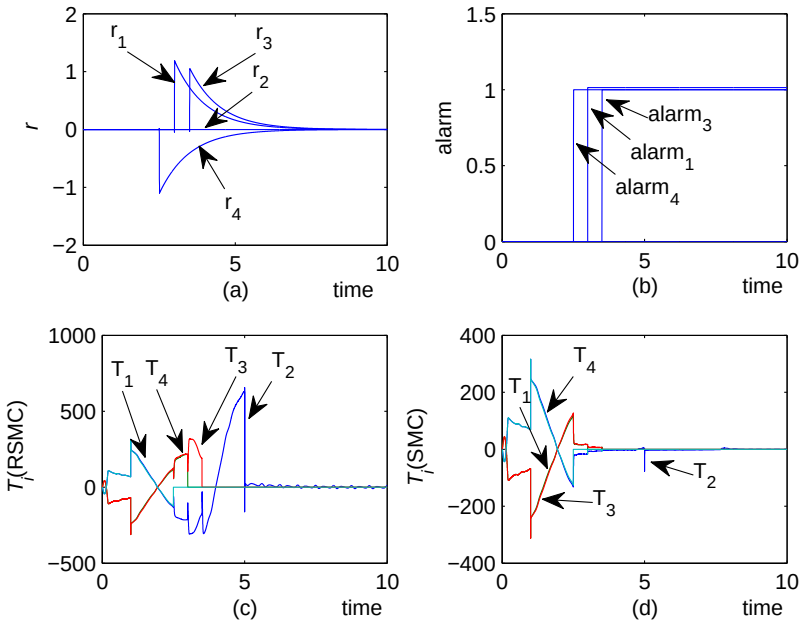

Fig. 4.12. (a) Residual signals; (b) alarm signal; (c) controls of RSMC and (d) Controls of SMC for three actuator faults.

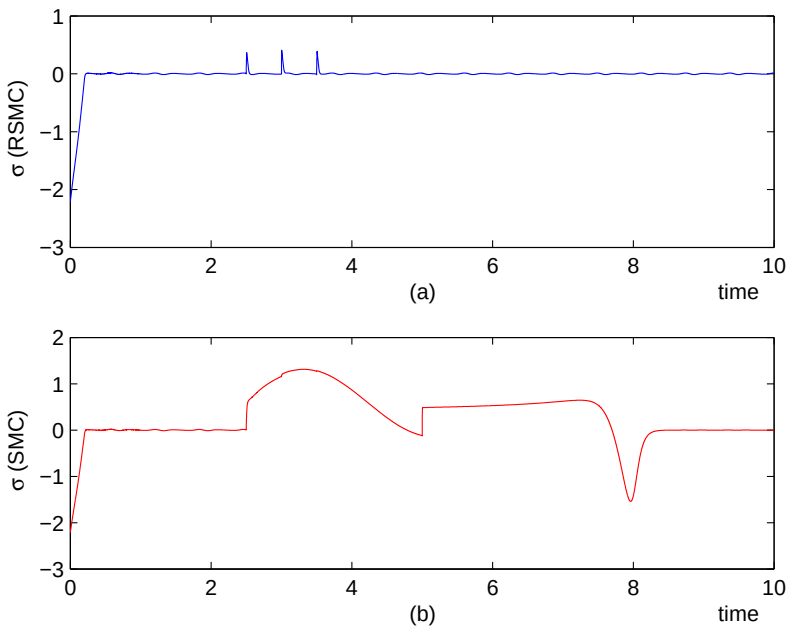

Fig. 4.13. Sliding variables of (a) RSMC and (b) SMC schemes for three actuator faults.

CHAPTER FIVE
CONCLUSIONS AND SUGGESTIONS FOR FURTHER RESEARCH

A combined scheme using the SDRE design for a nominal system and the ISMC strategy for model uncertainties and/or disturbances has presented. This combined scheme is shown to be able to preserve the same state response as that of the SDRE scheme for the nominal system when the uncertainties are of the matched type. We also apply these analytical results to a three-wheeled vehicle brake control system. The results demonstrate that the combined scheme has the ability to intelligently adjust the steering angle and the wheel torques so that the yaw rate and lateral velocity are the same as those of the nominal system under the SDRE scheme. Hence, the combined scheme is more effective and robust than using the SDRE scheme alone, thereby greatly enhancing the braking safety. It is also worth noting that the engineers may adopt any other optimal control strategy (other than the SDRE scheme) in accordance with the nominal system requirements to create a desired state trajectory for the uncertain system to follow.

In this thesis, we also have presented a class of SMC-type reliable controllers to generate a suitably yaw moment for EVs' yaw rate tracking task. These reliable controllers are shown to be able to successfully track the desired yaw rate when the vehicle experiences some of the actuators' faults. The body side slip angle can also be maintained in a small magnitude which depends on the desired yaw rate and steering command. Besides, the vehicle model under investigation is nonlinear rather than linear one, and the proposed reliable controllers do preserve the advantages of SMC design, including robustness, ease of implementation and responding rapidly. Simulation results have shown the effectiveness and benefits of the design.

To further extend the research covered in this thesis, we note several directions:

- Consider the situation of actuator total failure and the case of unmatch type uncertainties and/or external disturbances.
- Choose suitable D_s in the ISMC design to enhance system performance.
- Apply the combined scheme to other practically physical systems.
- Track both the body side slip angle and yaw rate simultaneously to improve the vehicle safety for lane change task.

References

[1] T. Acarman, "Nonlinear optimal integrated vehicle control using individual braking torque and steering angle with on-line control allocation by using state-dependent Riccati equation technique," *Vehicle System Dynamics*, vol. 47, pp. 155-177, 2009.

[2] M. Amodeo, A. Ferrara, R. Terzaghi, and C. Vecchio, "Wheel slip control via second-order sliding-mode generation," *IEEE Trans. Intelligent Transportation Systems*, vol. 11, pp. 122-131, 2010.

[3] M. Canale, L. Fagiano, A. Ferrara, and C. Vecchio, "Comparing internal model control and sliding-mode approaches for vehicle yaw control," *IEEE Trans. Intelligent Transportation Systems*, vol. 10, pp. 31-41, 2009.

[4] W. Cho, J. Yoon, S. Yim, B. Koo, and K. Yi, "Estimation of tire forces for fpplication to vehicle stability control," *IEEE Trans. on Vehicular Technology*, vol. 59, pp. 638-649, 2010.

[5] W. J. Cao and J. X. Xu, "Nonlinear integral-type sliding surface for both matched and unmatched uncertain systems," *IEEE Trans. Automatic Control*, vol. 49, pp. 1355-1360, 2004.

[6] F. Castanos and L. Fridman, "Analysis and design of integral sliding manifolds for systems with unmatched perturbations," *IEEE Trans. Automatic Control*, vol. 51, pp. 853-858, 2006.

[7] T. Cimen, "State-Dependent Riccatif Equation (SDRE) Control: A Survey," in: *Proc. of the 17th IFAC World Congree*, Seoul, Korea, vol. 17, pp. 3761-3775, 2008.

[8] P. E. Dumont, A. Aitouche, R. Merzouki, and M. Bayart, "Fault tolerant control on an electric vehicle," *Proc. Int. Conf. Ind. Techno.*, Singapore, 2006, pp. 2450-2455.

[9] R.A. Decarlo, S.H. Zak, and G.P. Matthews, "Variable structure control of nonlinear multivariable systems: A tutorial," IEEE Proc., pp. 212-232, Mar. 1988.

[10] E. Esmailzadeh, A. Goodarzi, and G. R. Vossoughi, "Optimal yaw moment control law for improved vehicle handling," *Mechatronics*, vol. 13, pp. 659-675, 2003

[11] C. Geng, L. Mostefai, M. Denai, and Y. Hori, "Direct yaw-Moment control of an in-wheel-motored electric vehicle based on body slip angle fuzzy observer," *IEEE Trans. on Industrial Electronics*, vol. 56, pp. 1411-1419, 2009.

[12] T. R. Gawade, S. Mukherjee, and D. Mohan, "Six-degree-of-freedom three-wheeled-vehicle model validation," *Proceedings of the Institution of Mechanical Engineers Part D-Journal of Automobile Engineering*, vol. 219, pp. 487-498, 2005.

[13] J. Huang and C.-F. Lin, "Numerical approach to computing nonlinear control laws," *J. Guid. Control Dyn.*, vol. 18, pp. 989-994, 1995.

[14] A. Harifi, A. Aghagolzadeh, G. Alizadeh, and M.Sadeghi, "Designing a sliding mode controller for slip control of antilock brake systems," *Transportation Research Part C-Emerging Technologies*, vol. 16, pp. 731-741, 2008.

[15] Y. Hori, "Future vehicle driven by electricity and Control-research on four-wheel-motored "UOT electric march II"," *IEEE Trans. Industrial Electronics*, vol. 51, pp. 954-962, 2004.

[16] U. Kiencke and L. Nielsen, *Automotive Control Systems for Engine, Driveline, and Vehicle*, Springer Verlag, Berlin, 2000.

[17] V. Kucera, "A contribution to matrix quadratic equations," *IEEE Trans. Automatic Control*, vol. 17, pp. 344-347, 1972.

[18] D. Kim, S. Hwang, and H. Kim, "Vehicle stability enhancement of four-wheel-drive hybrid electric vehicle using rear motor control," *IEEE Trans. Vehicular Technology*, vol.57, pp. 727-735, 2008.

[19] W. K. Lennon and K. M. Passino, "Intelligent control for brake systems," *IEEE Trans. Control Systems Technology*, vol. 7, pp. 188-202, 1999.

[20] L. Li, F.-Y. Wang, and Q. Zhou, "Integrated longitudinal and lateral tire/road friction modeling and monitoring for vehicle motion control," *IEEE Trans. Intelligent Transportation Systems*, vol. 7, pp. 1-19, 2006.

[21] Y.-W. Liang and S.-D. Xu, "Reliable control of nonlinear systems via variable structure scheme," *IEEE Trans. Automatic Control*, vol. 51, pp. 1721-1725, 2006.

[22] Y.-W. Liang, S.-D. Xu, and C.-L. Tsai, "Study of VSC reliable designs with application to spacecraft attitude stabilization," *IEEE Trans. Control Systems Technology*, vol. 15, pp. 332-338, 2007.

[23] Y.-W. Liang, S.-D. Xu, and L.-W. Ting "T-S model-based SMC reliable design for a class of nonlinear control systems," *IEEE Trans. Industrial Electronics*, vol. 56, pp. 3286-3295, 2009.

[24] F. Liao, J.L. Wang, and G.-H. Yang, "Reliable robust flight tracking control: An LMI approach", *IEEE Trans. Control Syst. Technol.*, vol. 10, no. 1, pp. 76-89, Jan. 2002.

[25] Y.-W. Liang, S.-D. Xu, T.-C. Chu, and C.-C. Cheng, "Reliable output tracking control for a class of nonlinear systems," *IEICE Trans. on Fundamentals of Electronics Communications and Computer Sciences*, vol. E87A, pp. 2314-2321, 2004.

[26] Y.-W. Liang, S.-D. Xu, and C.-L. Tsai, "Study of VSC reliable designs with application to spacecraft attitude stabilization," *IEEE Trans. Control Systems Technology*, vol. 15, pp. 332-338, 2007.

[27] Y.-W. Liang, D.-C. Liaw, and T.-C. Lee, "Reliable control of nonlinear systems," *IEEE Trans. Autom. Control*, vol. 45, pp. 706-710, Apr. 2000.

[28] Y.-W. Liang and S.-D. Xu, "Reliable control of nonlinear systems via variable structure scheme,"*IEEE Trans. Autom. Control*, vol. 51, pp. 1721-1725, Oct. 2006.

[29] D. -C. Liaw, H. -H. Chiang, and T. -T. Lee, "Elucidating vehicle lateral dynamics using a bifurcation analysis", *IEEE Trans. Intelligent Transportation Systems*, vol. 8, pp. 195-207, 2007.

[30] G. F. Mauer, "A fuzzy logic controller for an ABS braking system," *IEEE Trans. Fuzzy Systems*, vol. 3, pp. 381-388, 1995.

[31] C. P. Mracek and J. R. Cloutier, "Control designs for the nonlinear benchmark problem via the state-dependent Riccati equation method," *International Journal of Robust and Nonlinear Control*, vol. 8, pp. 401-433, 1998.

[32] J. S. Shamma and J. R. Cloutier, "Existence of SDRE stabilizing feedback," *IEEE Transactions on Automatic Control*, vol. 48, pp. 513-517, 2003.

[33] V. I. Utkin, *Sliding modes in control and optimizations*, Berlin, Germany, Springer-Verlag, 1992.

[34] I. Unger and R. Isermann, "Fault tolerant sensors for vehicle dynamics control," *Proc. Amer. Control Conf.*, Minneapolis, MN, 2006, pp. 3948-3953.

[35] R.J. Veillette, J.V. Medanic, and W.R. Perkins, "Design of reliable control systems," *IEEE Trans. Autom. Control*, vol. 37, pp. 290- 304, Mar. 1992.

[36] M. Vidyasagar and N. Viswanadham, "Reliable stabilization using a multi-controller configuration," *Automatica*, vol. 21, pp. 599-602, Sep. 1985.

[37] J. Y. Wong, *Theory of Ground Vehicles*, Wiley, pp. 57-63, 2008.

[38] W.D. Xiang, P. C. Richardson, C.M. Zhao, and S. Mohammad, "Automobile brake-by-wire control system design and analysis," *IEEE Trans. Vehicular Technology*, vol. 57, pp. 138-145, 2008.

[39] H. Yang, V. Cocquempot and B. Jiang "Optimal fault-tolerant path-tracking control for 4WS4WD electrical vehicles," *IEEE Trans. Intelligent Transportation Systems*, vol. 11, pp. 237-243, 2010.

[40] Y. Yamaguchi and T. Murakami, "Adaptive control for virtual steering characteristics on electric vehicle using steer-by-wire system, *IEEE Trans. Industrial Electronics*, vol. 56, pp. 1585-1594, 2009.

[41] H. Yang, V. Cocquempot and B. Jiang, "Optimal fault-tolerant path-tracking control for 4WS4WD electric vehicles," *IEEE Trans. Intelligent Transportation Systems*, vol. 11, pp. 237-243, 2010.